SCUOLA INTERNAZIONALE SUPERIORE DI STUDI AVANZATI

SISSA Digital Library

Extracting limits on dark matter annihilation from gamma ray observations towards dwarf spheroidal galaxies

note finali coverpage

(Article begins on next page)

01 May 2024

Extracting limits on dark matter annihilation from gamma-ray observations towards dwarf spheroidal galaxies

Ilias Cholis[1, 2, *] and Paolo Salucci[1, 2, †]

[1] SISSA, Via Bonomea, 265, 34136 Trieste, Italy
[2] INFN, Sezione di Trieste, Via Bonomea 265, 34136 Trieste, Italy
(Dated: November 14, 2012)

Dwarf spheroidal galaxies compose one of the most dark matter dominated classes of objects, making them a set of targets to search for signals of dark matter annihilation. Recent developments in γ-ray astronomy, most importantly the launch of the *Fermi*-LAT instrument, have brought those targets into attention. Yet, no clear excess of γ-rays has been confirmed from these targets, resulting in some of the tightest limits on dark matter annihilation from indirect searches. In extracting limits from dwarf spheroidal galaxies, it is of great importance to properly take into account all relevant uncertainties. Those include the dark matter distribution properties of the dwarf spheroidals and the uncertainties on the underlying background. We revisit the limits on dark matter annihilation, from γ-rays studying a set of close-by dwarf spheroidal galaxies for which we have good understanding of the uncertainties in the dark matter distribution. For those targets, we perform and compare results for alternative methods in extracting the background γ-ray flux. This provides a method to discriminate among the dark matter annihilation targets, those that can give robust constraints. We finally present our tightest limits on dark matter annihilation that come only from the targets that ensure accurate understanding of both the γ-ray background and the dark matter distribution uncertainties.

I. INTRODUCTION

Dark matter (DM) composes approximately 85% of the matter density in the universe, yet its particle physics properties in the Weakly Interacting Massive Particle (WIMP) case still remain unknown. Measurements of cosmic rays (CR) [1–7] have generated new model building [8–22] and new constraints on dark matter properties[23–27]. Also, direct detection experiments [28–33] have provided their own set of constraints (or preferred regions) on the mass and interaction properties of DM particles with nucleons [34–40] (see also [41–43]), providing possible insights on DM properties [44–49]).

Recently strong constraints on DM annihilation have been put from observations at γ-rays towards dwarf spheroidal (dSph) galaxies [50, 51]. DSph galaxies are DM dominated objects, where the production of γ-rays from point sources and from interactions between CRs and the local medium is expected to be suppressed. This supresion are due to the fact that baryonic gas densities are very low, star formation responsible for the producion of CRs is suppressed and also because CR escape timescales from those galaxies are expected to be much smaller compared to galaxies of sizes similar to that of the Milky Way. Thus, dSphs provide some of the best targets to look for signals from DM annihilation [52–57], that could possibly be probed with the current γ-ray telescopes.

Let us consider a galaxy in which DM annihilates producing γ-rays. In that case the relative flux is given by[150]

$$\frac{d\Phi_\gamma}{dE} = \int\int \frac{\langle\sigma v\rangle}{4\pi}\frac{dN_\gamma}{dE}_{DM}\frac{\rho_{DM}^2(l,\Omega)}{2\,m_\chi^2}dld\Omega, \tag{1}$$

where $d\Omega$ is the solid angle within which the measurement is done, and l the length along the line of sight to the object. For a homogeneous annihilation cross-section eq. 1 can be simplified to $d\Phi_\gamma/dE = \Phi^{PP}J$ where

$$\Phi^{PP} = \frac{\langle\sigma v\rangle}{4\pi}\frac{dN_\gamma}{dE}_{DM}\frac{1}{2\,m_\chi^2} \tag{2}$$

is a factor depending only on the elementary particle physics underlying the annihilation of the DM particles with mass m_χ, annihilating with a cross-section $\langle\sigma v\rangle$ and producing a spectrum of γ-rays per annihilation given by $\frac{dN_\gamma}{dE}_{DM}$.

---

*Electronic address: ilias.cholis@sissa.it
†Electronic address: salucci@sissa.it

The J-factor:

$$J = \int \int \rho_{DM}^2(l,\Omega)dld\Omega, \tag{3}$$

gives the line of sight integral of the DM density-squared over the solid angle $d\Omega$ under which the measurement is done.

Since limits from dSphs are on the $d\Phi_\gamma/dE$ from each dSph galaxy, the limits on DM annihilation cross-section depend strongly on the DM profile assumptions for those dSphs, i.e the J-factors as we describe in section II. The ρ_{DM} profile inserted for the calculation of the J-factors must be that obtained from observations from those dSphs. Over the past decade, observations have provided detailed information about the distribution of DM within the regions of spiral galaxies where the baryons reside ([58, 59]), suggesting a preference towards cored profiles for the dwarf spheroidal galaxies, rather than NFW profiles. Since the J-factors depend on the ρ_{DM}^2, the choice on an NFW or in general a cuspy profile (rather than a cored profile), may have an impact on suggesting greater values on the J-factors.

Also, since no clear excess towards dSphs has been observed, it is equally important to understand the γ-ray background contribution. The γ-ray background spectrum is composed of the isotropic component -which is the sum of the extragalactic γ-ray background and misidentified CRs-, the diffuse γ-rays produced in our Galaxy from CR interaction with the interstellar medium (ISM), and also of point sources laying inside the observation window/Region of Interest (ROI). In section III we discuss various methods of calculating residual γ-ray spectra at the location of the dSphs (that come from subtracting the modeled γ-ray backgrounds from the total fluxes), and suggest alternative methods. In section IV we further study individually eight dSph galaxies and the quality/robustness of the limits on DM annihilation based on the alternative methods of extracting residual spectra. Finally, in section V we present the strongest and most robust conservative limits on DM annihilation from dSphs and give our conclusions in section VI.

II. J-FACTORS

In disk systems the ordered rotational motions and the known geometry of the tracers of gravitational field facilitate the mass modeling. Moreover, in dwarf galaxies the DM emerges clearly. It has been shown that the fraction DM/Luminous matter increases with radius and at a fixed radius it increases with decreasing luminosity [60]. [58] it has suggested that the stellar disks are "maximal" and embedded in dark matter halos with a *cored* density distribution [58](see also [61–64]. Furthermore, there appear scaling relations between the structural properties of the luminous and of the dark mass components, [65–67]. In fact, results from the universal Rotaion Curve and individual Rotation Curves (RCs) of galaxies, [59, 68] imply that in galaxies the DM halo has a Burkert density profile:

$$\rho(r) = \frac{\rho_0\, r_0^3}{(r+r_0)\,(r^2+r_0^2)}, \tag{4}$$

in which the two free parameters, the core radius r_0 and the central halo density ρ_0 are related. In other words RCs of spirals and of Low Surface Brightness (LSB) galaxies yield a mass towards distribution that can be uniquely modeled by means of a luminous and a cored dark matter component. [59].

The knowledge of the mass distribution in pressure-supported systems like ellipticals and dwarf spheroidals is much more uncertain. The Local Group dwarf spheroidals galaxies (dSphs) occupy the faint end of the luminosity function of pressure-supported systems, [69, 70]. Their vicinity to us makes them the best candidates for the detection of possible γ-ray emission arising from annihilating dark matter, in thier densest parts. However, deriving the dSph mass model is not an easy task both observationally, in terms of measuring in each dSph a sufficiently large number of meaningful relative velocities of stars, and also from a dynamical modeling point of view, due the lack of precise information on the dynamical state of the latter. On the other hand, dSphs are simple systems and are DM dominated at all radii that are at least two orders of magnitudes less luminous than the faintest spirals [71]. The DM halo typically outweighs the baryonic matter by a large factor (from a few tens, up to several hundred). No dark-visible (potentially uncertain) mass decomposition is then needed to derive the DM properties. Also, there is evidence of universality in the DM halo structural properties of dSph galaxies [72] [73–76], in tension with the collision free particles of the naive ΛCDM scenario.

The study of the kinematics of the Milky Way dSphs has been revolutionized by multi-object spectrographs on 4m and 8m-class telescopes. Large data sets comprising between several hundred and several thousand individual stellar velocities per galaxy, have now been acquired for all the most luminous dSphs surrounding the Milky Way [70, 74, 77–79]. For these objects reliable measurements of the (projected) dispersion velocity profile are now available, so that a mass model can be attempted [74, 78–80]. It is well known that the dSph kinematics can be made compatible with the gravitational potential of the cuspy DM halos out of cosmological N-body simulations in the ΛCDM scenario (e.g.,

[81]). On the other hand, the same kinematics are also compatible with shallower DM profiles [76]. The point being that in dSphs the kinematics alone (e.g. the velocity dispersions) cannot discriminate among the various DM density profiles. The Jeans equation that relates the density and the velocity dispersion of the stellar component to the mass profile of the dark matter halo has a well-known degeneracy between the mass profile and the velocity anisotropy profile (see for instance[74, 79, 82]). In spite of these difficulties, cored DM profiles seem to be favored in very recent studies, [71, 73, 79, 83–85]. However, also in these cases, cuspier NFW profiles cannot be ruled out.

The situation for dwarf spirals is very different. These objects, DM dominated down to their inner regions, have very reliable kinematics from their stellar and gaseous disks that, unambiguously point towards centrally flat density dark matter halos. The kinematics commonly suggest a cored profile as is a Burkert profile or a similarly shallow one. As a matter of fact, for dwarfs spirals we can state that the NFW halo velocity profile under no circumstances can reproduce their rotation curve [86].

Of equal importance is the fact that in the evolution of DM density in dSphs strong outflow events occur (due to some strong early supernovae explosions), that suppress the baryonic infall at later stages. This mass loss and input in the dSph galaxies is claimed to have largely modified the cosmological NFW DM halo profile that has emerged from N-Body DM-only simulations in the ΛCDM scenario [87, 88], to shallower profiles.

For these reasons, in the estimate of the J factor in nearby dSphs, which is the first step of constraining the mass and cross section of annihilating dark matter, it is unjustified to assume that the dSphs have dark matter halos following the NFW profile. On this line [89] have investigated the internal kinematics of the Milky Way dSphs, by first taking the usual assumption that the luminous component consists of a single pressure-supported stellar population in dynamical equilibrium; therefore tracing the underlying gravitational potential. [89] also assumed that the latter is dominated by the dark matter halo, leading to uts density profile to be easily traced by the Jeans equation, given by:

$$\nu(r)v_r^2 = Gr^{-2\beta} \int_r^\infty s^{2\beta-2}\nu(s)M(s)ds. \tag{5}$$

In order to use observables, the stellar component must be projected along the line of sight [90]:

$$\sigma_p^2(R) = \frac{2}{I(R)} \int_R^\infty \left(1 - \beta(r)\frac{R^2}{r^2}\right) \frac{\nu(r)v_r^2(r)r}{\sqrt{r^2 - R^2}} dr, \tag{6}$$

where $I(R)$ is the projected stellar density profile and $\sigma_p(R)$ is the projected velocity dispersion profile which are both known. $M(r)$ is the mass profile of DM, $\nu(r)$ describes the 3-dim stellar distribution and $v_r(r)$ is the radial velocity of the stars. The orbital anisotropy $\beta(r)$ is not constrained, as all information about the velocity distribution is restricted to the component along the line of sight. [89] did the simplifying assumption that $\beta = $ constant, which provides the following solution to eq. 6 [91], and then use in eq. 6 rather than the NFW mass/density profile, that derived for a Burkert halo [59].

$$
\begin{aligned}
M(r) &= 4\pi \int_0^r s^2\rho(s)ds \\
&= 2\pi\rho_0 r_0^3 \left(\ln[(1 + r/r_0)] + 0.5\ln[(1 + r^2/r_0^2)] - \tan^{-1}[r/r_0]\right).
\end{aligned} \tag{7}
$$

Here the two DM structural parameters are its central density and its core radius. In short [89] *assumed* a cored profile to represent the DM halo, allowed a radially constant velocity anisotropy different for every object and aimed to reproduce the observed dispersion profiles as closely as possible. In detail [89] obtain (marginalized) 1-D posterior probability distribution functions for each of the two DM profile free parameters using a Markov-Chain Monte Carlo (MCMC) algorithm leading to "best fits" values for these parameters. These results demonstrate that Burkert profiles can provide an excellent description of dSph velocity dispersion profiles and that the available data quite well constrain the structural parameters. In Table 2 of [89] the authors provide the individual values of r_0, ρ_0 and their best fit uncertainties for eight galaxies, which we study in the following.

The reliability of the derived mass model is also given by the fact that although the DM densities in dSphs are about two orders of magnitude higher than those found in (larger) disc systems (by comparison to the stellar ones), their DM halos best fit values for the structural parameters lay on the extrapolation (at lower masses), of the same r_0 and ρ_0 relationship found to hold for spirals and ellipticals [92]:

$$r_0 = 8.6(\rho_0/(10^{23}gcm^{-3})^{-1}kpc \tag{8}$$

We note that based on eq. 8 the error propagation of the two quantities are not statistically independent. The product of $\rho_0 r_0$ varies at most by 50% in galaxies [92]. This uncertainty is the major source of uncertainty in the

dSph	D (kpc)	δD (kpc)	l	b	$\overline{J} \times 10^{17}$ ($GeV^2 cm^{-5}$)	$\delta J_{high} \times 10^{17}$ ($GeV^2 cm^{-5}$)	$\delta J_{low} \times 10^{17}$ ($GeV^2 cm^{-5}$)	α_c
Carina	103	4	260.1	-22.2	2.69	0.47	0.54	$0.27°$
Draco	84	8	86.4	34.7	29.2	7.52	5.84	$0.27°$
Fornax	138	9	237.1	-65.7	5.66	1.38	1.51	$0.56°$
LeoI	247	19	226.0	49.1	3.07	1.00	1.51	$0.11°$
LeoII	216	9	220.2	67.2	3.98	8.11	3.52	$0.08°$
Sculptor	87	5	287.5	-83.2	18.3	4.08	3.85	$0.42°$
Sextans	88	4	243.5	42.3	23.6	58.3	17.2	$0.89°$
Ursa Minor	74	12	105.0	44.8	25.0	18.9	17.7	$0.49°$

TABLE I: Dwarf Spheroidal galaxies used in this analysis. For the J-factors we give the mean value from the fit of [89] $\overline{J}$ and the upper and lower 1 σ uncertainties δJ_{high}, δJ_{low}, all evaluated within an angle of α_c.

evaluation of the J-factors for the targets calculated at α_c (given in table I) and defined as:

$$\alpha_c = \frac{2\overline{r_{half}}}{D}, \tag{9}$$

with $\overline{r_{half}}$ being the half light radius of the stellar population in the dwarf and D it's distance to us. The induced uncertainty in the J-factor from uncertainty of the distance D from us is subdominant by comparison.

We refer to the original paper of [89] for details but it is worth to discuss explicitly the role played by velocity anisotropy in the derived modeling. Under the assumption of Burkert haloes for dSphs the inclusion of velocity anisotropy as a free parameter improves the quality of the dispersion profile fits relative to those obtained for isotropic models. However, [89] we also find that the scatter in the ρ_0-r_0 relation is smaller for anisotropic models, thus the better we reproduce the observed dispersion profiles using Burkert haloes, the tighter is the correlation between the halo parameters.

In Fig. 1 (upper plot) we give the results on the J-factors from [89] versus the best fit value for the central density. There is a clear correlation between the uncertainty on the value of the J-factor and the best fit value for ρ_0, where larger values for ρ_0, are related to larger uncertainty on the evaluated $J(\alpha_c)$. We note that both the uncertainties and the ρ_0 value, come from the MCMC fit to the data, i.e. the velocity dispersion profiles for the eight dwarf spheroidal galaxies. Yet, such a correlation is not a complete coincidence. Given that all dSphs lay at $\rho_0 r_0 \approx const.$ (our eq. 8), larger ρ_0 result in lower values of r_0 and $\overline{r_{half}}$. Thus smaller in size DM halos. For the larger DM halos the stars distributed in the inner part and generally within the inner kpc (see [89]) [151], probe better the inner part of the actual DM halo profile, which results in smaller uncertainties for the J-factors.

In Fig. 1 (bottom) we also compare the results of [89] which are our reference results for the J-factors, to those of [51] and [93]. As is clear, [51] has a tendency in assuming smaller uncertainties in the J-factors than [89] and [93] do. Such an assumption can influence the strength of the limits on DM annihilation rates, on top of the fact that in [51] a cuspy NFW profile has been used.

Finally, we want to emphasize that the results of [89], do not *require* the presence of cored haloes in dSphs, nor do they constrain the density and scale lengths of their haloes in a model-independent way. On the other hand, the fact that the dSph kinematics can be reproduced using Burkert DM halo profiles whose structural parameters lie on the same scaling relations as those of spirals, provides support for the assumption that the mass distributions in dSph galaxies has the same framework of those of spirals. This can replace the idea that the dSph follow the profiles arising from N-Body simulations in LCDM scenario. [152]

Let us stress that in previous works, faint objects like Segue I have been used to constrain WIMP masses and cross sections. However, for these objects, presently, we do not have a dispersion velocity profile of their stellar component, but only a measure of an "average" dispersion, that, in addition cannot even be attributed to a particular radius. Therefore, for them, an analysis of investigating different mass profiles has no meaning. A single measurement at an unspecified radius does not allow us to build a reliable mass model, even by taking a number of assumptions. Since we have no way of estimating the total dark mass, let alone the DM distributions, of Segue I, Ursa Major II and Coma Berenices, we leave them for future work.

III.   FERMI GAMMA-RAY DATA

In [50, 51, 93, 94], it has been suggested that no clear excess of γ-rays between 200 MeV and 100 GeV (above the expected background) has been measured towards known dwarf spheroidal galaxies. Thus strong constraints on the DM annihilation can be placed. Yet, since the expected DM signal is smaller than the modeled background, the exact assumptions made to calculate the background γ-rays can be crucial in finding or hiding a DM signal.
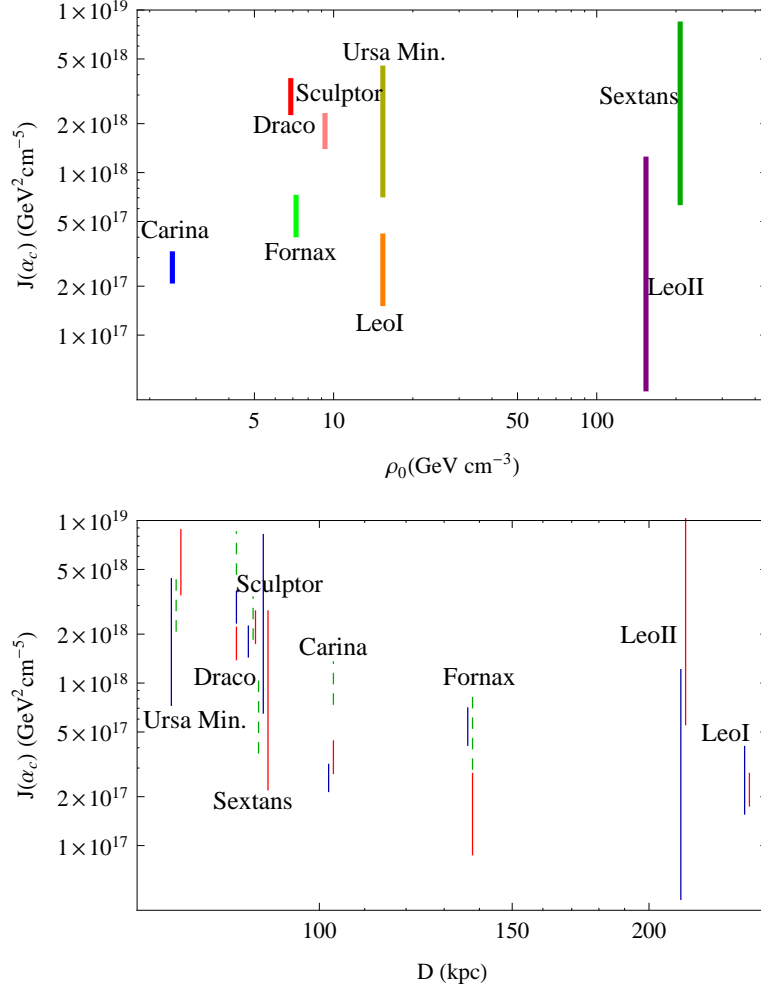
FIG. 1: *Top*: The *J*-factor at α_c vs the best fit value for ρ_0 from [89]. *Bottom*: Comparison between J-factors in that work: *dark blue* (from [89]),in the work of [93]: *red* and the assumptions of [51] (recalculated within α_c): *dashed green*.

Since we want to set conservative limits on DM annihilation, we will ignore a possible contribution to the γ-ray flux from each dSph from other sources of γ-rays in the dSph, considering that the entire γ-ray flux from each dSph comes from annihilating DM. Yet in the same angular window there is background flux from unrated sources unrated to the dSphs. This γ-ray background originates from the galactic diffuse γ-rays, the isotropic γ-ray background, the contribution of nearby point sources and finally from CRs misidentified for γ-rays. At lower energies different sources can overlap with the possible contribution from the dSph due to the poorer angular resolution of the *Fermi* LAT instrument at low energies. The CRs contribution can vary based on different selection criteria of γ-ray events (event class). Using tighter criteria on the selection of γ-ray events, a cleaner sample can be achieved at the expense of lower statistics [153]. As mentioned in the introduction, we study the effects on the induced limits on the DM annihilation, from different assumptions around in modeling the γ-ray background around each target, and in choosing different classes of γ-ray events.

According to the *Fermi* LAT site [154], there are three classes of events that can be used for γ-ray analysis, the "SOURCE", the "CLEAN" and the "ULTRACLEAN" classes of events, with the SOURCE class having the highest contamination of CR events (among those three classes) and the ULTRACLEAN the lowest. We will use all three classes to derive excess γ-ray fluxes from the direction of the targets. We will also study the effects in choosing different combinations of Regions Of Interest (ROI), for the γ-ray flux of each dSph target and its relevant γ-ray background. In our analysis we used 3 years of data taken between Augist 2008 and August 2011 with the PASS7 classes criteria.

We will first use the SOURCE class of events as was done by the *Fermi* Collaboration in [50, 51], with the analysis provided in the Fermi ScienceTools[155]. In [51] for every dSph of interest an initial ROI of 10° radius centered at each

target was selected. Then a binned Poisson likelihood fit was performed "to both spatial and spectral information in the data" [51], using $10°$ square spatial maps at energies between 200 MeV and 100 GeV. In those fits, the normalizations of the isotropic diffuse and the galactic diffuse γ-ray components *were left free in all ROIs*, and so where the normalizations of the point sources within $5°$ from the dSph.

We point out that in a region of $10° \times 10°$ where as we show in Table I (see α_c), all dSph are practically point sources[156] and thus their size is defined by the PSF at each relevant energy, choosing to vary the normalizations of the two diffuse components and the close-by point sources, can lead in hiding any DM signal and thus lead to strong constraints on DM annihilation. In fact, the *Fermi* Collaboration has released the Isotropic Diffuse Gamma-Ray spectrum [95], with an analysis on the expected contamination from CRs for different cuts on events. Thus instead of allowing the isotropic diffuse component to vary, one should use a *fixed* spectrum that would be the sum of the Extra Galactic Background γ-ray spectrum as has been also given in [95], and the CR contamination spectrum relevant for the SOURCE class of events. Regarding the galactic diffuse component, we know it is the sum of γ-rays produced from π^0 decays and to a smaller extend decays of other mesons produced at $p-p$, $p-He$, $He-p$, $He-He$ collisions between CRs and the ISM targets, bremsstrahlung off CR $e^\pm$ interacting with the ISM gas and up-scattering of CMB and the interstellar radiation field photons from CR $e^\pm$. Its contribution within each ROI should also come from a fixed physical model such as those done in [96, 97] where also agreement with CR measurements has been confirmed and not with the galactic diffuse model of "gal_2yearp7v6_v0" that is let also to have a free normalization in the minimization fit. The same arguments apply also to the point sources normalizations and pawer-laws (which are also let free).

Moreover, these targets of annihilating DM are expected to be strongly subdominant components of γ-rays below $E_\gamma \sim$ GeV for the case of WIMP masses $m_\chi \approx 10$ GeV. As a result including in the analysis data bellow 1 GeV that have by far more statistics than above 1 GeV will let the fit to be dominated by the low energy data. Just the 1σ errors on the flux at low energies whether statistical fluctuations or of systematic origin, will be significant in suggesting the presence or absence of residuals at high energies where the DM signal may lie. An example of a possible systematic error at low energies would be, a dim point source with a hard spectrum and a cut-off at $E_\gamma \sim 1$ GeV, as are millisecond pulsars (MSPs) [98] that has not been included (being not a known source), such a source could cause a fluctuation to the low energy data. MSPs has been observed to have a spectrum given by:

$$\frac{dN_\gamma}{dE} \sim E^{-\Gamma} e^{-E/E_c}, \tag{10}$$

with $\Gamma = 1.5 \pm 0.4$ and $E_c = 2.8 \pm 1.9$ GeV and luminosity in γ-rays of $L = 10^{33.9 \pm 0.6}$ erg/s [98]. In the Galaxy their contribution to the EGBR is expected to be $O(0.1)$ [99, 100] between 0.5 and few GeV giving a flux of:

$$E^2 \frac{dN_\gamma}{dE} \approx 5 \times 10^{-4} \, MeV \, cm^{-2} s^{-1} sr^{-1}, \text{ between 0.1 and 10 GeV.} \tag{11}$$

Following the assumptions of [101] that would lead to a population of $\sim 10^4$ MSPs in the entire sky. That makes the probability of one unidentified MSP within a region of $10° \times 10°$ to be $O(1)$ even if their distribution in the sky is not truly isotropic since they are galactic sources. We clarify also that the large scale distribution properties and the impact of the averaged spectral properties of the MSP has been included in the combination of the Isotropic and galactic diffuse template components that are fitted to the actual γ-ray data. Yet the combination of these components can not account for all posible structures in the γ-ray events, which is the reason why, after all they have been used in the searches for unknown point sources [102, 103].

The case for detecting a DM signal may be even more difficult for light DM cases where both the DM and the backgrounds have their main contribution at low energies, with the backgrounds though, being dominant. We note also that below 1 GeV the containment angle of the *Fermi* LAT instrument is $> 1°$ ($> 3°$) at 68% (95%) at normal incidence for PASS7 SOURCE and CLEAN class data (P7SOURCE_V6, P7CLEAN_V6), thus the dSphs are dimmed even further at low energies by having their luminosity below 1 GeV being spread at a wider angle.

For all these reasons we are concerned that the contribution of dim DM point-like sources can be hidden by a background with many available degrees of freedom in the minimization procedure, and thus lead to very tight constraints on annihilating DM from each dSph. For a significantly brighter source as those detected by the *Fermi* LAT, [102–104] that may not be as much of an issue, since also for their joint optimization analysis there are many more ROIs (there are 1873 point sources in the 2 yr catalogue [103]) sharing data and the information of already known point sources [103].

We want to also note that in [51] a joint likelihood analysis was done, where 10 ROIs where combined. As is written in the "Data Analysis" section of [51], the normalizations of the nearby point sources and of the diffuse gamma-ray sources as well as the J-factors of the dSphs are among the "ROI-dependent model parameters", i.e. [51] still allow for freedom in the normalizations of the diffuse components, something that is certainly wrong for the isotropic one which is also the most important at high latitudes where many of these targets lay (see Fig. 2).
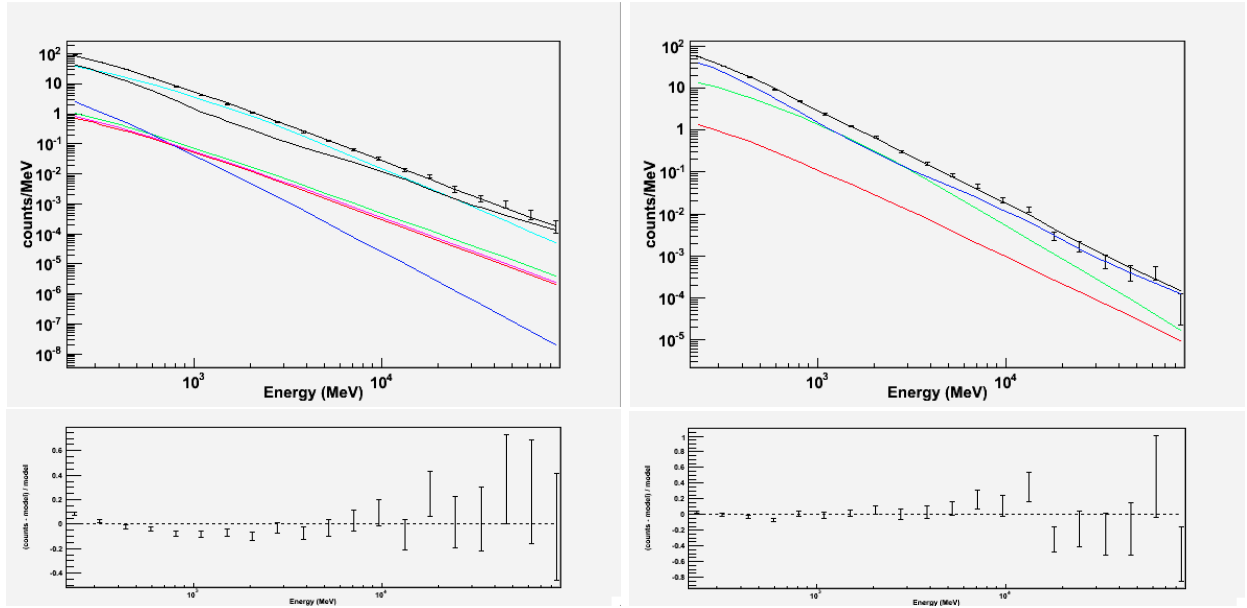
FIG. 2: Total (counts/MeV) and residual (counts-model)/model spectra from the minimization procedure of Fermi tools P7. We used SOURCE class data within $5°$ from the relevant dSph position, and within energies of 200 MeV and 100 GeV (separated in 20 energy bins). *Left*: Draco, where apart from the isotropic and the galactic diffuse components, four known point sources contribute within $5°$. *Right*: Sculptor, where one point source has been detected.
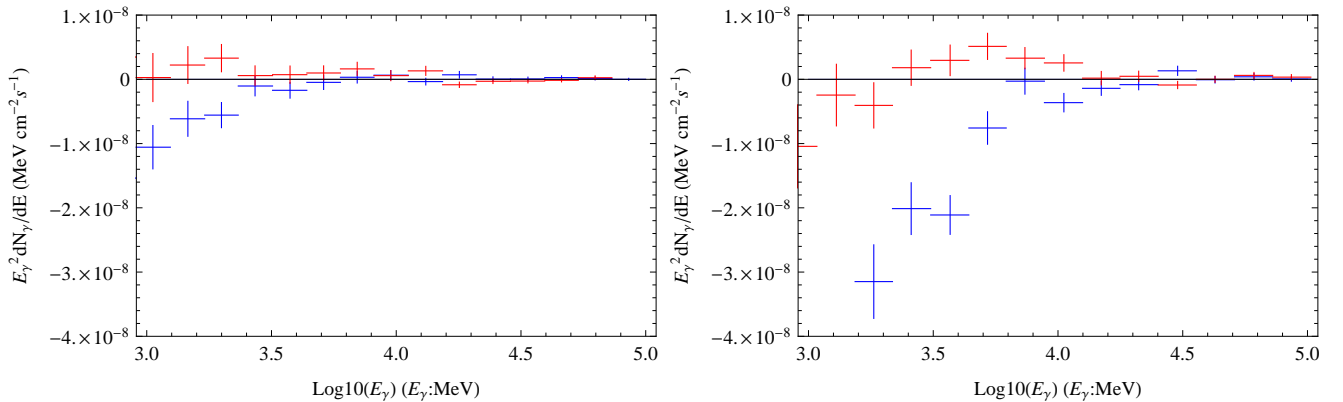

FIG. 3: Excess gamma-ray differential flux for Draco (dark blue) and Sculptor (red) dwarf spheroidal galaxies, using *Fermi* data "SOURCE" class. We present the spectra between 1 GeV and 100 GeV. *Left:* Using in the minimization procedure all data between 200 MeV and 100 GeV, within a radius of $5°$, as presented in Fig. 2. *Right:* Using all data between 100 MeV and 100 GeV, within a radius of $10°$

Finally we point out that the joint likelihood analysis is made to account for uncertainties in the J-factors of the dSphs, which in fact can still not correct for a possible systematic bias towards higher values of J-factors coming from assuming an NFW DM profile.

As an example using the publicly available *Fermi* ScienceTools we calculated the residual spectra shown in Fig. 2 and 3 for Draco and Sculptor with all the relevant point sources within $5°$ from each dSph galaxy. For Draco which is one of the targets that provides the strongest limits on DM annihilation cross-sections, there are 4 relevant point sources (see top left of Fig. 2).

As a test to the sensitivity of the minimization procedure that gives residual spectra we used the region of the sky centered at Draco (not including the DM contribution from Draco) and decided to add one by one the known point sources from brightest to dimmest (defined by the fit when all known sources are included). Such a choice of a test can be motivated by the possibility of some yet undetected point source contributing to the total γ-ray flux within the ROI. We also decided to change the angle where the minimization is carried from $5°$ to $10°$, where 15 point sources have been discovered. We also increased minimally the energy range for the minimization, from 200-10^5 MeV

ROI	E_{min} (MeV)	# of P.S.	N_{GDM}	F_{GDM} ($\times 10^{-4}$)	N_{iso}	F_{iso} ($\times 10^{-4}$)	N_{J1725}	α_{J1725}
5°	200	1 p.s.	1.458 ± 0.041	4.160 ± 0.118	0.830 ± 0.032	0.697 ± 0.028	-	-
5°	200	4 p.s.	1.403 ± 0.042	4.001 ± 0.121	0.803 ± 0.036	0.674 ± 0.030	4.00 ± 0.58	-2.526 ± 0.14
10°	200	1 p.s.	1.574 ± 0.021	4.489 ± 0.060	0.795 ± 0.016	0.669 ± 0.014	-	-
10°	200	10 p.s.	1.426 ± 0.021	4.068 ± 0.060	0.781 ± 0.017	0.655 ± 0.014	4.12 ± 0.59	-2.31 ± 0.14
10°	200	15 p.s.	1.406 ± 0.007	4.012 ± 0.020	0.775 ± 0.005	0.650 ± 0.005	4.00 ± 0.43	-2.25 ± 0.10
10°	100	1 p.s.	1.582 ± 0.017	7.617 ± 0.084	0.903 ± 0.011	1.871 ± 0.022	-	-
10°	100	10 p.s.	1.462 ± 0.018	7.058 ± 0.086	0.871 ± 0.012	1.804 ± 0.024	3.49 ± 0.53	-2.40 ± 0.16
10°	100	15 p.s.	1.474 ± 0.018	7.120 ± 0.087	0.842 ± 0.014	1.744 ± 0.029	3.29 ± 0.58	-2.19 ± 0.17
5°	200	4 p.s.	1.192 ± 0.018	3.401 ± 0.052	1.000 ± 0.000	0.839 ± 0.000	3.69 ± 0.58	-2.12 ± 0.13
10°	200	15 p.s.	1.157 ± 0.003	3.301 ± 0.008	1.000 ± 0.000	0.839 ± 0.000	3.70 ± 0.21	-2.10 ± 0.04
10°	100	15 p.s.	1.274 ± 0.009	6.150 ± 0.043	1.000 ± 0.000	2.071 ± 0.000	3.03 ± 0.57	-2.02 ± 0.14

TABLE II: Galactic Diffuse Model (GDM):"gal_2yearp7v6_v0", Isotropic Model (iso):"iso_p7v6source", J1725 refers to the specific point source (see text). F_{GDM} and F_{iso} are in units of ph cm^{-2}s^{-1}, from the specific region of interest. N_{GDM}, N_{iso} and N_{J1725} are normalizations for the equivalent spectral components.

to 100-10^5 MeV within the 10° radius case; in order to check the sensitivity of the results on varying the relevant assumptions. Finally we have fixed the normalization of the isotropic component to 1 and for different choices of ROI and energy range redone the fit. For every case we give in Table II the normalizations of the isotropic diffuse, the galactic diffuse and the normalization and index for the closest to Draco detected point source J1725.2+5853 ("J1725")[157] that come from the fit, using the ScienceTools. As can be seen the normalization of the galactic diffuse and the isotropic diffuse can have a change between fits of $O(0.1)$, which is far more than the residual signal. Thus we conclude that the method for analyzing the residual spectra from dSphs as is done by the *Fermi* Collaboration makes assumptions that are not generically valid, and there is a need for alternative methods.

The target of our analysis is to use an alternative method to study the possible DM signal from dSph galaxies addressing the following issues:

- Model the background for each dSph in a method that does not allow for many degrees of freedom that could result as stated above in hiding any small excess.

- Minimize the dependence on the possibility of other undetected point sources existing in the ROI (unless they happen to overlap with the dSph location).

- Avoid having low energy γ-rays dominate our results.

- Include the fact that the *Fermi* LAT instrument has a PSF that depends on energy.

- Minimize the significance of CR contamination, which at high latitudes and energies can be important.

- Avoid having too low statistics.

In our method for every dSph galaxy and energy bin we choose 2 regions of interest. One contains the dSph centered at it's location which for simplicity we will refer to as "signal ROI(s)". The other in that energy bin does not contain the dSph but is used to measure the γ-ray background of the dSph referred to as "background ROI(s)". The signal ROIs include the region of the sky defined by a radius of angle α_1. The background ROIs are defined in the most general case by two radii, α_2 and α_3 and include the region of the sky defined as $\alpha_2 < \alpha < \alpha_3$ from the center of each dSph. As we will describe later, we will test various combinations of α_1, α_2, α_3 in order to ensure that our criteria set above are met. We have tested cases where $\alpha_1 \leq \alpha_2$ as shown in Fig.4. For all dSphs and at each energy bin we subtract from the averaged γ-ray flux of the signal ROI the averaged γ-ray flux of the equivalent background ROI.

We stress that the background γ-ray flux to each dSph at a given energy bin is the γ-ray flux at that energy bin between $\alpha_2 < \alpha < \alpha_3$, and is kept fixed thus no additional d.o.f. for the background model are allowed. Similar methods are common in gamma-ray astronomy [105–107] and in general[108–111]. Furthermore the isotropic flux contribution which is the dominant component in most cases, and includes the EGBR and the CR contamination is in our method subtracted[158] (without adding a freedom in it's normalization). Also, since our choices for the sizes of the ROIs are similar to that of [50, 51] any contribution from undetected point sources is taken into account. An other characteristic of our analysis is that regarding claims of positive (excess) or negative residual γ-ray fluxes, each energy bin is independent from the others. This does not let the lower energy bins with the higher statistics influence the search for a possible residual γ-ray flux at higher energies.

We clarify that for background ROIs extending too far away from the dSphs one includes into the background flux the contribution of sources (e.g. point sources or emission from ISM gas) that are irrelevant to the actual background
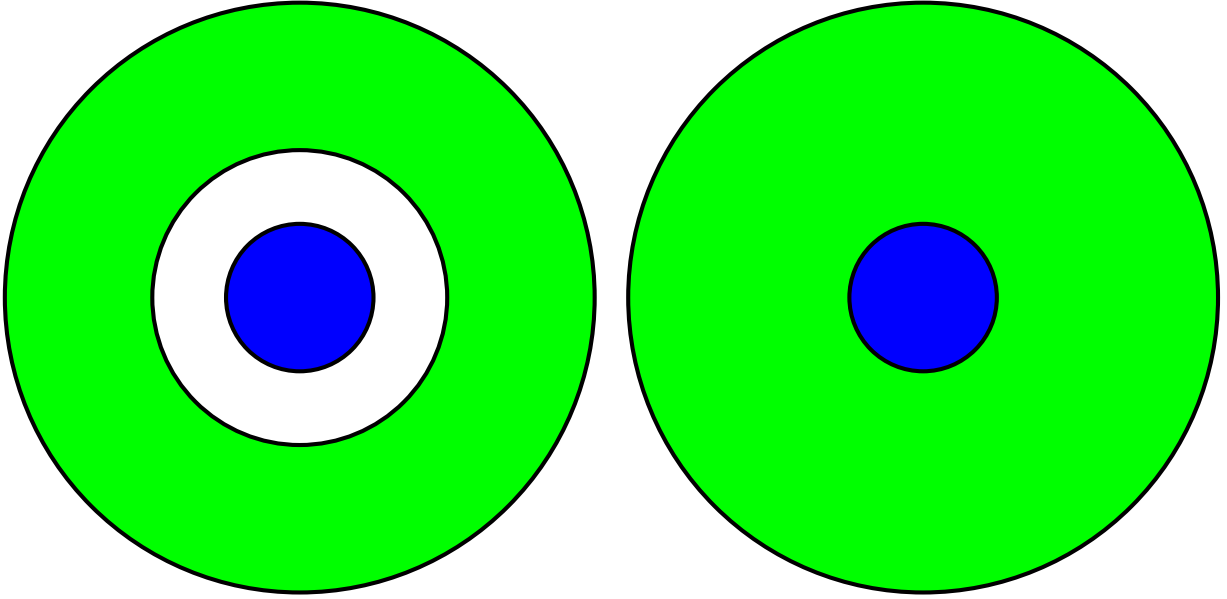
FIG. 4: Signal *blue*(central disk) and Background *light green*(outer ring) Regions Of Interest for versions 1 to 4 *left*, and versions 5 to 6 *right*.

γ-ray flux at the location of the dSphs. Thus while we show also some results from more extended background ROIs we will focus on these choices where proximity to the target is ensured.

Since we want to take into account the PFS vs E_γ information, while at the same time avoid having our analysis on the DM limits be dominated by low energy γ-rays, we choose to use $E_\gamma \geq 1$ GeV and up to 100 GeV. At $E > 100$ GeV the low statistics and the noise of the contamination of CRs becomes a concern. To minimize contamination from CRs, we use for the rest of our analysis either the CLEAN or the ULTRACLEAN class of events. At $E < 1$ GeV the PSF becomes too large, which in our method has the disadvantage of having the region of the sky where the dSph does not contribute being too far from the center of the dSph. That results in the signal ROI being very large, and thus the background ROI is too far from the center of the dSph, to provide a proper model for the background γ-ray spectrum. We break the 1-100 GeV range in 6 logarithmically equally spaced energy bins, giving in theory a total of 12 ROIs for each target and for the entire energy range. As we will explain later though, the ROIs for the last three energy bins are always the same, setting the actual number of ROIs per target to be 8.

We clarify that such an analysis is not optimized for low mass DM. As we explained earlier in the text, in our opinion the low mass DM cases can not be probed in dSphs with an instrument whose PSF containment angle is significantly larger than the target sizes at the relevant energies where the DM annihilation signal lies.

For each energy bin we will take as the relevant angular size of the object in the sky $\alpha_{dSph}(E)$, either α_c, or the 95% containment angle at normal incidence at approximately the center of the energy bin, depending on which of the two is the largest. Thus we treat the smallest in size (on the sky) dSphs as practically point sources and the largest ones as extended sources. For our selection of dSphs apart from Sextans at energies above 10 GeV α_{dSph} is defined by the containment angle.

For our analysis α_{dSph} will set either α_1 or α_2 at each bin, given in Table III. The most important remaining issue is that of low statistics at higher energy bins. In Table III we present our assumptions for α_1, α_2 and α_3. We show in Fig. 5 the residual spectra for the four targets that give the tightest limits on DM annihilation rates, for the case where $\alpha_1 < \alpha_2$ (versions 1 to 4), using the CLEAN data set.

In Fig. 6 we present for Ursa Minor the residual spectra using, equivalently CLEAN and ULTRACLEAN data. There is not much gain in using the cleanest of the two samples and thus to avoid having too low statistics we use for the remaining work the CLEAN selection class.

In Fig. 7 we show the residual spectra for the case of $\alpha_1(E) = \alpha_2(E) = \alpha_{dSph}(E)$, with α_3 being 5° (version 5) or 10°(version 6). While with version 6 we extend the background ROI out to 10°, ensuring smaller statistical errors for the background, the additional angular area (5°-10° from the dSph center) used in calculating the background results in decreasing the relevance of the calculated background to the actual background flux at the location of the dSph. That can result in significant changes of the residual spectra at the lower energy bins, as is most clear for the cases of Draco and Sextans dSphs. Since the signal ROIs for both versions 5 and 6 are identical, the origin is strictly
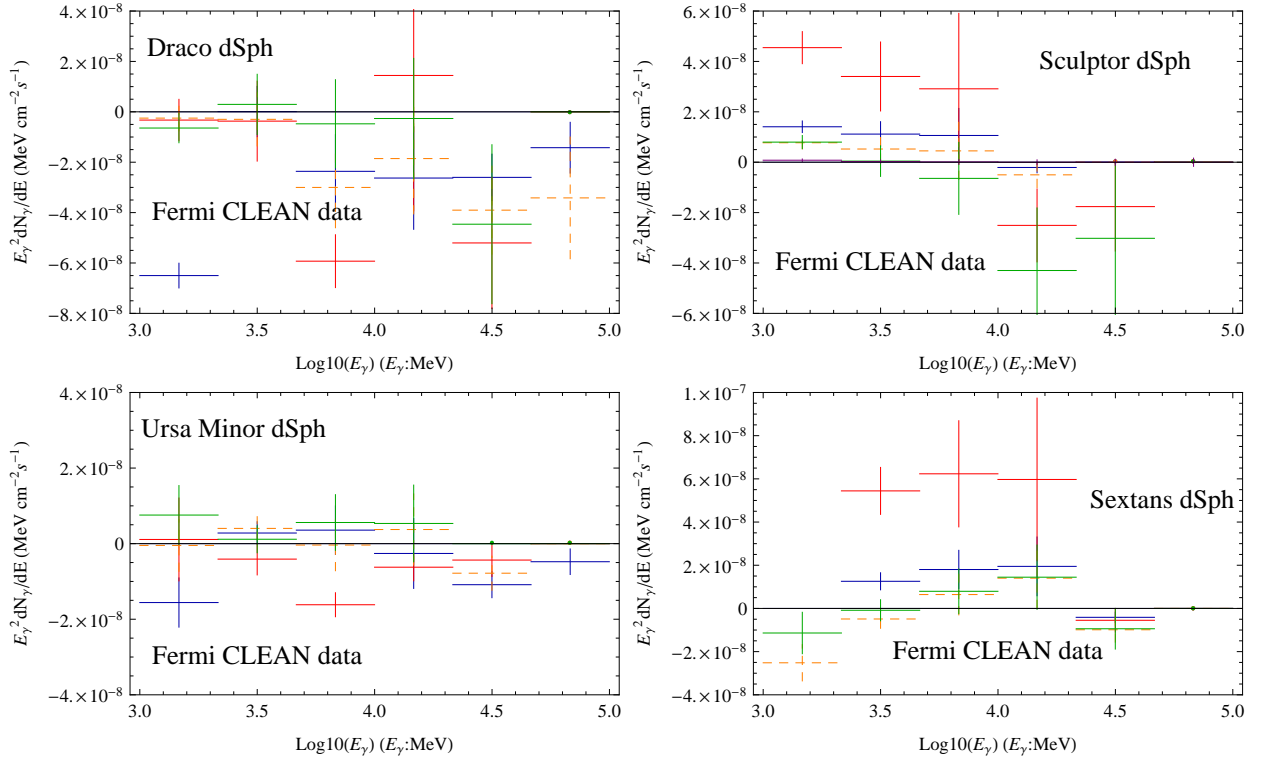
FIG. 5: Excess gamma-ray differential flux for dwarf spheroidal galaxies, using *Fermi* data "Clean" class. *Upper left:* Draco, *upper right:* Sculptor, *lower left:* Ursa Minor, *lower right:* Sextans. Dark blue: version 1, red: version 2, dashed orange: version 3, green: version 4.
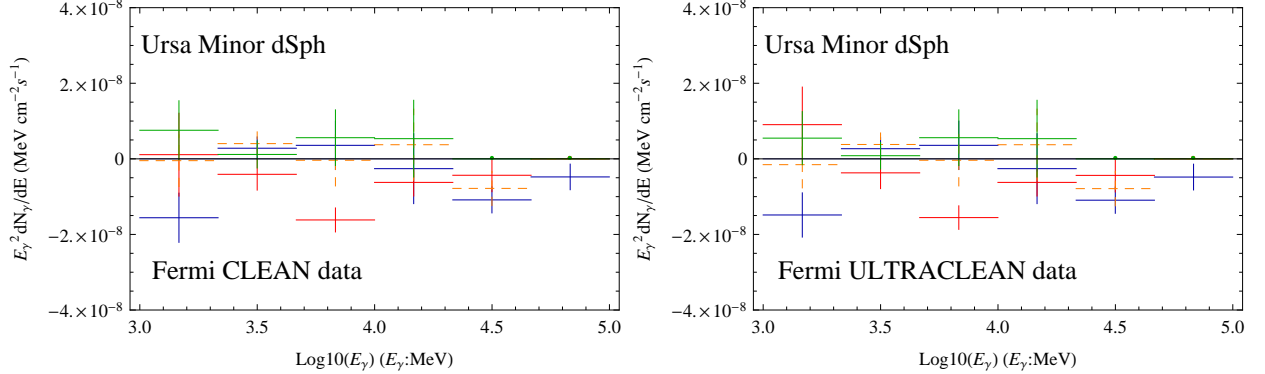

FIG. 6: Residual spectra from ROIs versions 1 to 4 for Ursa Minor using CLEAN *left* and ULTRACLEAN *right* event selection. Colors as in Fig. 5.

from the background calculation. That difference is mainly due to the fact that for these targets the relevant flux from the point sources centered within 5° from the center of the dSph at study to the flux from the point sources centered within 10° changes significantly[159]. Point sources are expected to be more important at lower energies due to their softer spectrum (on average) compared to the isotropic and the galactic diffuse spectral components of the γ-ray background. Also at high energies where the PSF is bellow 1° extending the background region out to 10° can only be correct if the background at these energies is almost isotropic.

For these reasons we consider version 5 preferable to version 6, and thus while we show the residual spectra from version 6 in Fig. 7, we avoid including them further into our analysis. For the same arguments version 4 is preferable to versions 1 and 3. Version 2 assumes very small signal ROIs resulting in too low statistics, which in return gives systematically weaker constraints on annihilation rates. We will include versions 1-3 in some of our results, since at least at high energies they all use for the background regions that are not further than 5° away from the center of the

case	E_γ^{mean} (GeV)	E_γ^{min} (GeV)	E_γ^{max} (GeV)	α_1	α_2	α_3
Version 1	1.47	1.00	2.15	2.5°	5.0°	10.0°
	3.16	2.15	4.64	1.5°	3.0°	6.0°
	6.81	4.64	10.0	1.0°	2.0°	4.0°
	14.7	10.0	21.5	0.8°	1.6°	3.2°
	31.6	21.5	46.4	0.8°	1.6°	3.2°
	68.1	46.4	100	0.8°	1.6°	3.2°
Version 2	1.47	1.00	2.15	1.5°	2.5°	5.0°
	3.16	2.15	4.64	0.9°	1.5°	3.0°
	6.81	4.64	10.0	0.6°	1.0°	2.0°
	14.7	10.0	21.5	0.48°	0.8°	1.6°
	31.6	21.5	46.4	0.48°	0.8°	1.6°
	68.1	46.4	100	0.48°	0.8°	1.6°
Version 3	1.47	1.00	2.15	2.5°	5.0°	7.5°
	3.16	2.15	4.64	1.5°	3.0°	4.5°
	6.81	4.64	10.0	1.0°	2.0°	3.0°
	14.7	10.0	21.5	0.8°	1.6°	2.4°
	31.6	21.5	46.4	0.8°	1.6°	2.4°
	68.1	46.4	100	0.8°	1.6°	2.4°
Version 4	1.47	1.00	2.15	2.5°	3.75°	5.0°
	3.16	2.15	4.64	1.5°	2.25°	3.0°
	6.81	4.64	10.0	1.0°	1.5°	2.0°
	14.7	10.0	21.5	0.8°	1.2°	1.6°
	31.6	21.5	46.4	0.8°	1.2°	1.6°
	68.1	46.4	100	0.8°	1.2°	1.6°
Version 5	1.47	1.00	2.15	2.5°	2.5°	5.0°
	3.16	2.15	4.64	1.5°	1.5°	5.0°
	6.81	4.64	10.0	1.0°	1.0°	5.0°
	14.7	10.0	21.5	0.8°	0.8°	5.0°
	31.6	21.5	46.4	0.8°	0.8°	5.0°
	68.1	46.4	100	0.8°	0.8°	5.0°
Version 6	1.47	1.00	2.15	2.5°	2.5°	10.0°
	3.16	2.15	4.64	1.5°	1.5°	10.0°
	6.81	4.64	10.0	1.0°	1.0°	10.0°
	14.7	10.0	21.5	0.8°	0.8°	10.0°
	31.6	21.5	46.4	0.8°	0.8°	10.0°
	68.1	46.4	100	0.8°	0.8°	10.0°

TABLE III: Combinations of α_1, α_2, α_3 for versions 1 to 4 ($\alpha_1 < \alpha_2$) of evaluating residual spectra, and versions 5 and 6 ($\alpha_1 = \alpha_2$).

dSphs.

IV.   GETTING DIFFERENT LIMITS

Each of the methods described in section III, results in different calculated residual spectra, and thus in different limits on DM annihilation rates. The flux from DM annihilation is calculated as [160]:

$$\frac{d\Phi_\gamma^{\,i}}{dE}\bigg|_{dSph_{DM}} = \frac{\langle\sigma v\rangle}{4\pi}\frac{dN_\gamma}{dE}\bigg|_{DM}\frac{J^i}{2\,m_\chi^2}, \tag{12}$$

where the index i, refers to the energy range/bin at interest since the J-factors differ between bins:

$$J^i = \int\int dl d\Omega^i \rho_{DM}^2(l,\Omega). \tag{13}$$

$d\Omega^i$ is different for energy bins with different signal ROIs, in our limits from versions 1 to 5 (see discussion in sections II and III).
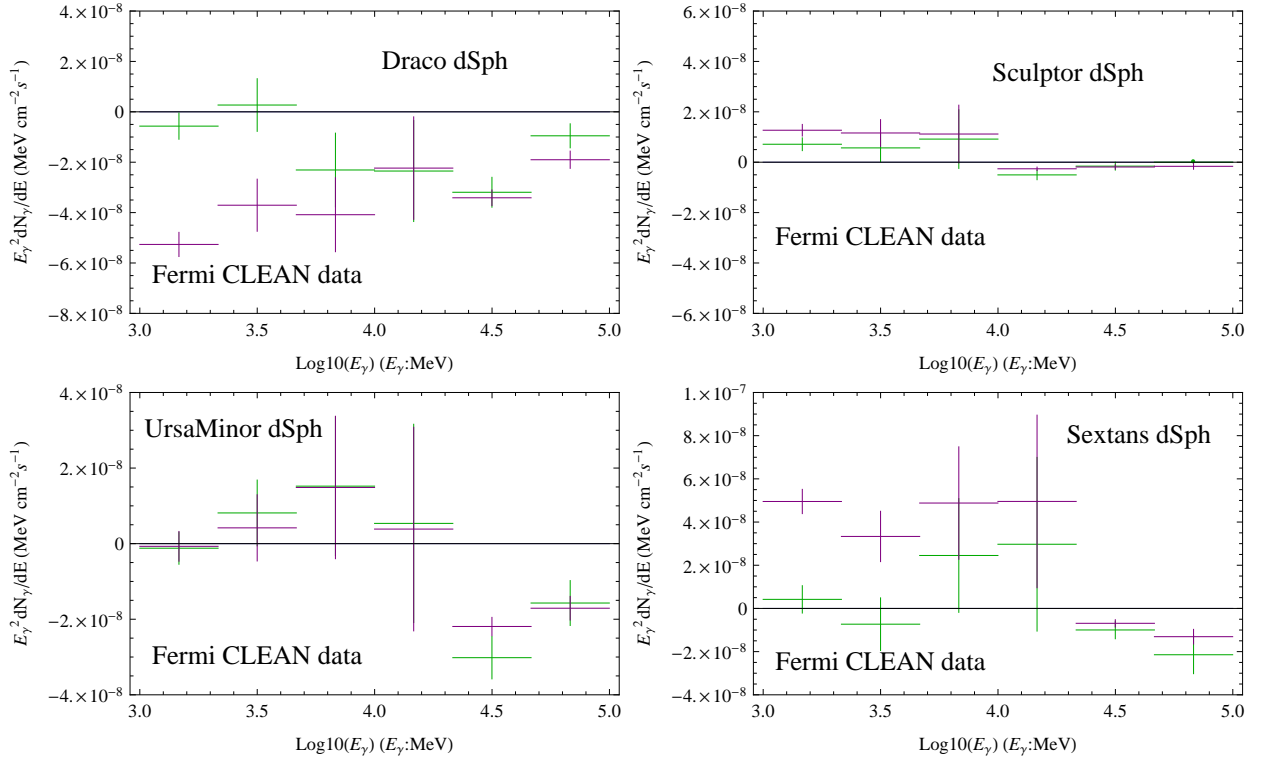
FIG. 7: Excess gamma-ray differential flux for dwarf spheroidal galaxies, using *Fermi* data "Clean" class. *Upper left:* Draco, *upper right:* Sculptor, *lower left:* Ursa Minor, *l ower right:* Sextans. Green: version 5, dark purple: version 6.

$\overline{J} \times 10^{17}$ $(GeV^2 cm^{-5})$	$\delta J_{high} \times 10^{17}$ $(GeV^2 cm^{-5})$	$\delta J_{low} \times 10^{17}$ $(GeV^2 cm^{-5})$	α
74.4	45.8	33.8	2.50°
72.7	39.6	32.3	1.50°
69.0	29.5	29.3	1.00°
65.3	22.3	26.3	0.80°
51.7	9.70	16.4	0.48°
29.2	7.52	5.84	0.27°

TABLE IV: The *J*-factor for Draco dSph with its upper and lower uncertainties for different containment angles α. The first four rows are relevant for versions 1, 3, 4 and 5 (see Table III). The fifth row is relevant for version 2, and the last row refers to the *J*-factor calculated at α_c (see Table I).

We clarify that the condition of Boost Factor, BF $= 1$ is for a thermally averaged annihilation cross-section of $\langle \sigma v \rangle = 3 \times 10^{-26} cm^3 s^{-1}$ in eq. 12 with the *J*-factors being *calculated for every energy bin* based on the $\alpha_{dwarf} = \alpha_1$. We give in Table IV the *J*-factors of Draco dSph within different containment angles α.

For a reference model of DM annihilation channel relevant for $\frac{dN_\gamma}{dE}_{DM}$ in eq. 12 ($\frac{dN_\gamma}{dE}_{DM}$ is the differential γ-ray spectrum per annihilation event) we consider the case of $\chi\chi \longrightarrow W^+W^-$, We take into account only the "prompt γ-rays" i.e. those that come from final state radiation and the hadronization processes after the decay of Ws. We used PYTHIA 6.4 [112] event generator to derive those γ-ray spectra. Ws can also decay into leptons by Branching Ratios of 0.1075 ± 0.0013 to e^+e^-, 0.1057 ± 0.0015 to $\mu^+\mu^-$, 0.1025 ± 0.0020 to $\tau^+\tau^-$ [113]. Some γ-rays will also be produced from inverse Compton scattering (ICS) by and bremsstrahlung radiation off the highly energetic $e^\pm$, that are among the stable final products. Yet these $e^\pm$ propagate from their original production point. Thus the relevant γ-ray components are more diffused, not directly related to the *J*-factors and less straightforward to calculate since one needs to add the information on the radiation field and the baryonic mass distribution in the form of gas and dust at the actual location of the dSphs. Since we know that dSphs have in mass a suppressed baryonic component, we expect the gas and dust number densities and the energy density of the radiation field at infrared and optical wavelengths to be suppressed compared to that in our Galaxy. Yet unless one carries a detailed analysis, for each dwarf spheroidal, one can not be confident that the hadronic channel giving prompt γ-rays is always the dominant
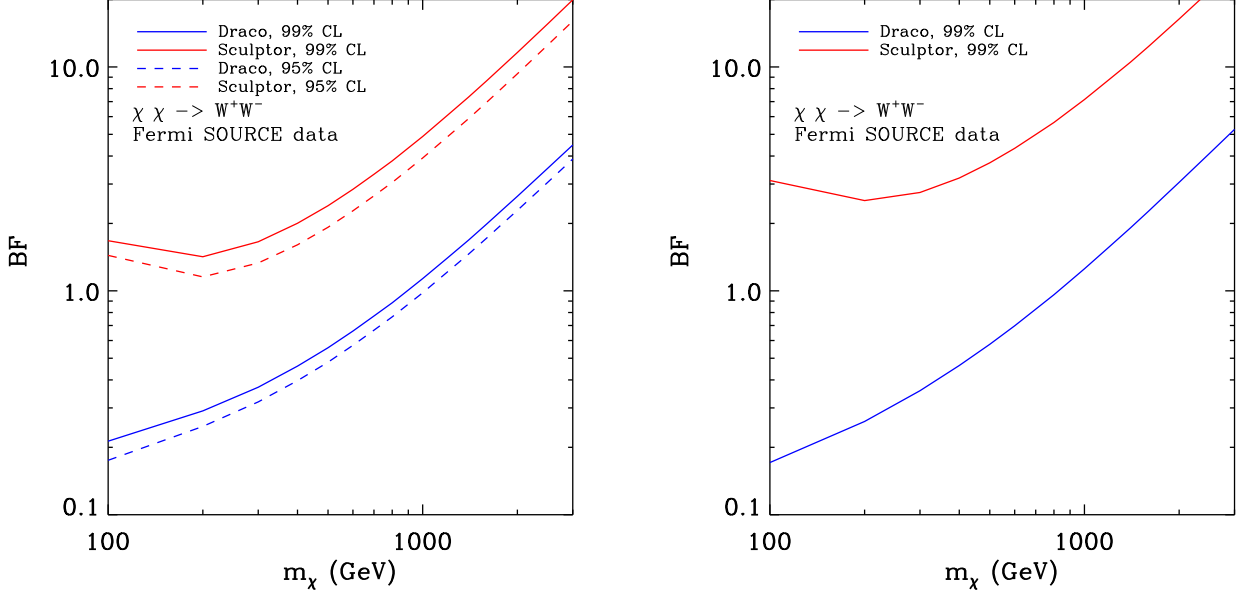
FIG. 8: 99% and 95% CL limits on annihilation rate for Draco (blue) and Sculptor (red) dwarf spheroidal galaxies. *Left*: using residual spectra of Fig. 3(left), with energy between 1 GeV and 100 GeV within 5°. *Right*: using residual spectra of Fig. 3 (right), within 10°.

part; especially for masses significantly larger ($\gtrsim 20$ times) than the energy range of the γ-ray data used [161]. Thus the reader should consider those limits as conservative ones. We also clarify that in our PYTHIA simulation we did not consider the decays of τs into π^0 and K^0s, which happens about $\approx 50\%$ of the time [113]. That last component is also a source of prompt γ-rays, which can though not change our results by more than $\approx 10\%$. For the case of the $\chi\chi \longrightarrow W^+W^-$ channel that we use here as reference, EW corrections [114] do not change our results (see also discussion in section V). Yet for more model dependent cases [115, 116], additional corrections are necessary.

In Fig. 8, we show the 95% and 99% CL limits on annihilation rate BF from Draco and Sculptor residual spectra (using the Fermi Tools only for the residual spectra) as shown in Fig. 2 and 3. To have a more direct comparison of the impact that our methods for the calculation of the residual spectra have on the DM BF limits, we used only the residual spectra between 1 and 100 GeV in 15 energy bins given also in Fig. 3. We calculate limits from both the cases where the data lay within 5° (Fig. 3 and 8 (left)) and within 10° (Fig. 3 and 8 (right)) from each dSph. For the limits of Fig. 8 since the ROI did not vary with E_γ we used the mean values and uncertainties from the case where $\alpha = 2.5°$.

As one can see from Fig. 8, the effect of different assumptions for the calculation of the residual flux can vary between targets and tends to give stronger constraints than our background models of version 4 and in some cases version 5 (shown in Fig. 9). Also for the case of 10° ROI, a DM signal from Draco and Sculptor is excluded at 95% CL.

In Fig. 9, we show the limits on DM annihilation rate, for our versions 4 and 5. We use as reference DM annihilating into W^+W^- as in Fig. 8. We show 68%, 99% and 99.9% CL limits from all eight dSphs at study. When lines are missing, that indicates that a DM annihilation signal for the given assumptions (DM mass, annihilation channel, and target assumptions) is excluded at the relevant CL. BF of less than 1 can be originating from an overestimation of the mean value of the J-factor, or an underestimation of the relevant error in calculating the J-factors (see discussion in section II). It can also be the case that DM annihilates to the relevant channel with a BR < 1, with the remaining channels of annihilation not giving a significant γ-ray signal at those energies.

In all cases the limits from the Draco dSph are the most stringent, with limits from Ursa Minor, Sextans, Sculptor and Fornax being the next most constraining set. Leo I, Leo II and Carina give limits systematically less stringent. That relevant power of dSph in setting limits on DM annihilation is also validated when using versions 1 to 3 (not shown here) and is also in rough agreement with results of other groups [50, 51, 93]. Yet the exact sequence of relative significance between dSphs changes between versions see for instance in Fig. 9 the relative change between Fornax and Sextans, and between Leo I and Carina.

We will consider that for our further discussion, it is enough to study the limits from four of those dSphs, namely
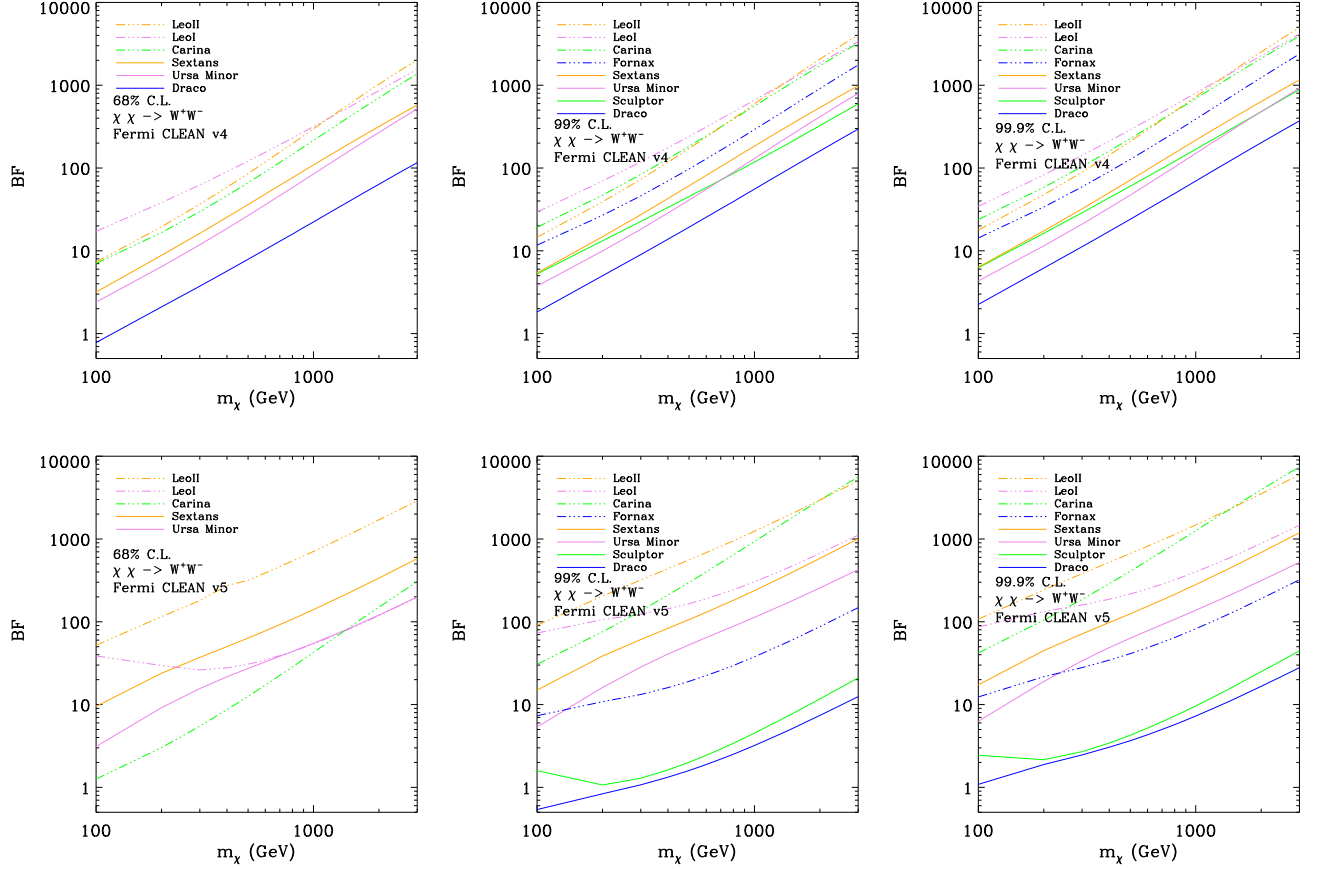
FIG. 9: Impact of different methods to estimate the background, on limits from dwarf spheroidals using *Fermi* CLEAN class of data. *Upper row*: using v4, *lower row*: using v5. *Left column:* 68% C.L., *middle column:* 99% C.L., *right column:* 99.9% C.L..

Draco, Ursa Minor, Sextans and Sculptor, for which the residual spectra from our various versions have also been given in Figs. 5-7. That choice is based both on the fact that these targets are more important in setting DM constraints and also because they provide a good subset of dSphs to show the issues that such an analysis on γ-ray data faces.

In Fig. 10 we show the limits on DM annihilation from these dSph galaxies, using the five different versions of deriving residual fluxes. While the limits from Draco dSph are more constraining as we show in Fig. 9, they vary significantly between different methods. In fact, for Draco, using our version 2 we even get to exclude DM annihilating to W^+W^- at 99% CL. Of interest is to consider what is the variation in the DM limits between version 4 (light green) and version 5 (dark green) in Fig. 10. Both versions assume the same set of signal ROIs, and consider background ROIs that as we described in section III ensure proximity to the targets. Yet the change in the exact set of background ROIs is enough to influence the limits on Draco between v4 and v5 by a factor of 4 at $m_\chi = 100 GeV$ to a factor of 20 at $m_\chi = 3 TeV$. Similar is the case with limits from Sculptor. On the contrary, Ursa Minor gives much more consistent limits between different versions, all of them agreeing within a factor of 3. Specifically versions 4 and 5 are consistent with each other by a factor of 2 or less. This fact suggests that while the limits from Ursa Minor are less constraining, they are much more robust. Finally Sextans, gives very robust limits at high masses (all versions agree within a factor of 3 for masses heavier than $m_\chi = 500$ GeV), but suggests greater relative differences in the DM limits at lower masses. Still even for Sextans our preferable versions 4 and 5, agree within a factor of 2 or less; proving an other target to derive robust limits.

There are various reasons why some targets provide more consistent limits than others when changing the background ROIs. One is that increasing the angular size of background ROIs point sources that may be far from the center of the dSph start having an impact. This is the case of Draco and Sextans at low E_γ. An other issue can be the existence of some structure in the galactic diffuse background within the ROIs, usually due to the presence of an ISM gas structure.

For the case of an ISM gas structure within the ROIs of interest, its contribution to the background γ-rays comes
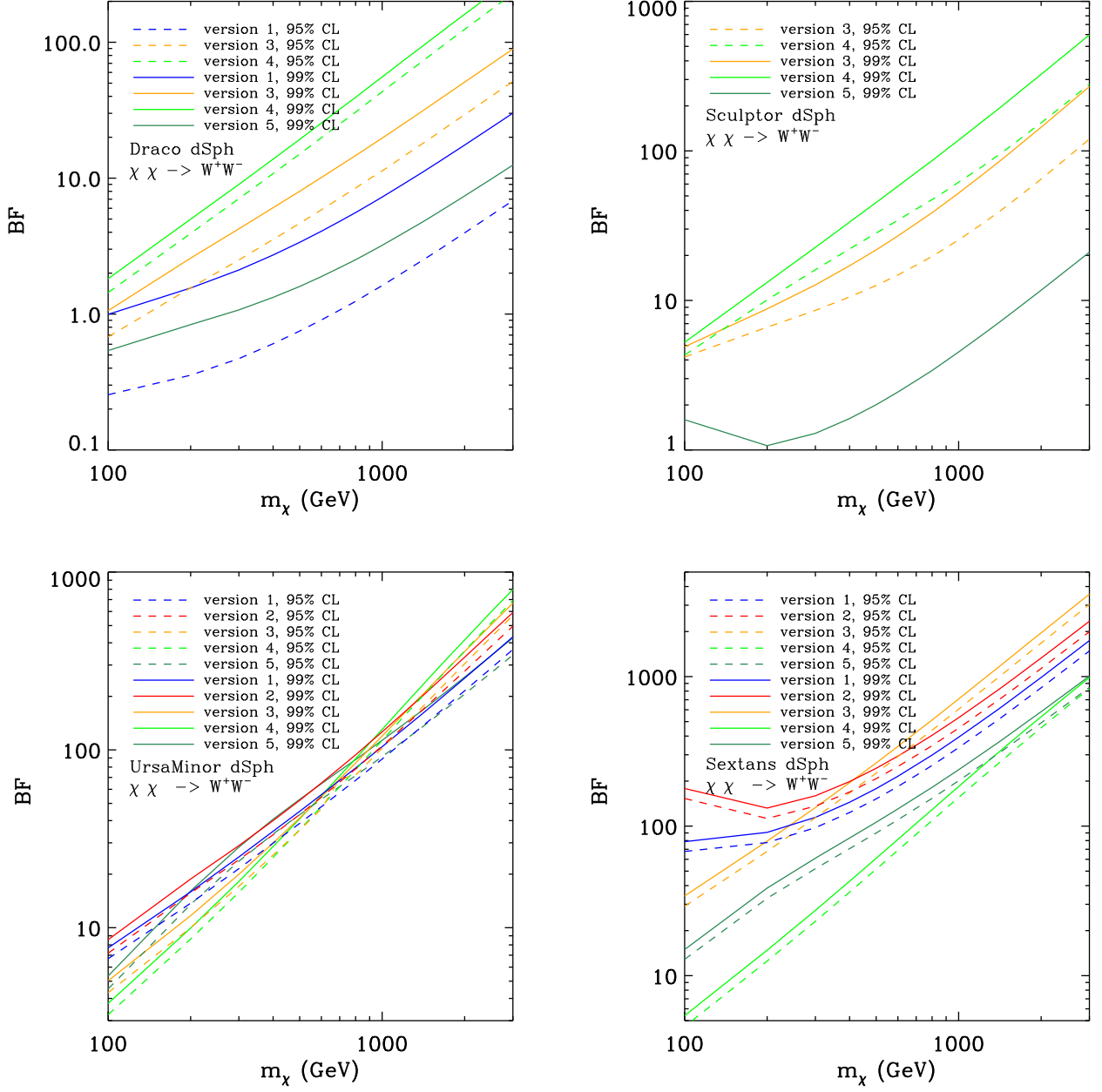
FIG. 10: 95% C.L. and 99% C.L. limits from dwarf spheroidals for versions 1-5 using *Fermi* CLEAN class data. *Upper left:* Draco, *upper right:* Sculptor, *lower left:* Ursa Minor, *lower right:* Sextans. For certain targets as Ursa Minor and Sextans, much more robust limits on DM annihilation can be achieved.

from bremsstrahlung off CR $e^{\pm}$ or pi0 (and other mesons) decay, produced from nucleon nucleon collisions (mainly pp) (see discussion in section III). To calculate that contribution, one needs to know the actual location of the gas in the Galaxy and to have a good understanding of CR density distribution in the Galaxy. The latter has been addressed in various works [96, 97, 117–119] where to ensure agreement with γ-ray data, large windows of the sky are used (for a recent analysis see [119]). The former, knowing the actual location of the gas structure is usually based on assumptions on rotation curves[96, 119–121] (or some velocity fields from stars motions[122]), which are generally correct for low latitudes since the gasses there are expected to follow well, the general motion. Yet at high distances from the galactic disk (and thus high latitudes), as are all the dSphs at study[162], the peculiar velocities of these ISM gasses can have a strong impact in setting their position in the Galaxy (see also discussion in [123]). Placing the small structures ISM gasses in the wrong position in the Galaxy (without changing its longitude and latitude coordinates),

would result in making wrong assumptions on the CR electron and proton density environment that these structures exist in. For instance the steady state CR protons density at $b = 30°$, may vary by a factor of 50% from moving a gas from 2 kpc to 4 kpc away from us (see [97] for cases of CR protons distribution profiles) [163].

The bremsstrahlung and pi0 components depend proportionally to the CR $e^{\pm}$ and the CR p densities (equivalently). Moreover the CR $e^{\pm}$ spectra due to fast energy losses, can vary significantly between different locations in the Galaxy. While these errors may seem insignificant we remind the reader that the residuals that we are in search of, are usually of $O(0.1)$ of the expected galactic diffuse component. Models such as that of [119] or the "gal_2yearp7v6_v0" while they can be consistent with γ-rays at large windows, can not be considered correct at small angular windows as those discussed.

The method of [51], that models the background components within the ROI, as discussed in section III, assumes too many degrees of freedom, since the p.s. flux normalizations and spectral power laws, the isotropic component normalization and galactic diffuse component normalization, are let to vary freely. The isotropic flux normalization should not be let to vary, especially between ROIs for different dSphs (see discussion III).

For those reasons we consider preferable to use in deriving limits from dSphs, only the targets that give consistent limits between versions 4 and 5 and for which we consider that the uncertainties in the J-factors are properly taken into account. From that class of targets the strongest limits come from Ursa Minor and Sextans.

An alternative method of analysis of the γ-ray data from these targets could be, masking out the point sources and the possible galactic features. Given that there are typically $O(100)$ γ-rays above 10 GeV within $5° - 10°$ window around these targets and for some targets like Draco $O(10)$ known point sources, such an analysis may not be optimal due to too few γ-rays remaining (especially for cases like Draco dSph). Yet that would be a question for a separate rigorous analysis.

V. CONSTRAINTS

Having shown in Fig. 10, versions 4 and 5 and using the W^+W^- channel as a guide, we notice that version 5 gives slightly weaker limits. In Fig. 11 we show the limits on DM annihilation BF only from version 5, for Ursa Minor (left column), and Sextans (right column). These limits are true conservative limits since apart from being slightly weaker than those of version 4, they come from targets that can give robust limits. These limits also come from a version that for the reasons described in section III addresses all the issues that can arise in calculating residual spectra and DM limits from dSphs. Finally, the limits are conservative, since we used only the prompt part of γ-rays from DM annihilations, including electroweak corrections [114, 124], but ignoring ICS from and bremsstrahlung off the $e^{\pm}$ that are also final products of DM annihilations in all the channels shown.

Apart from the $\chi\chi \longrightarrow W^+W^-$, in Fig 11 we give the 95% and 99% CL limits for general phenomenological channels as $\chi\chi \longrightarrow \tau^+\tau^-$, $\chi\chi \longrightarrow \mu^+\mu^-$, $\chi\chi \longrightarrow b\bar{b}$ and $\chi\chi \longrightarrow t\bar{t}$.

As is clear Ursa Minor gives stronger limits than Sextans by a factor of 2.5 at 1TeV to a factor of 4 at 10 GeV for all channels shown. Comparing our limits to those of [51] we get for Ursa Minor a factor of 5 stronger limits at 10 GeV and a factor of 2 at 1TeV. Although given that there is an uncertainty by a factor of 3 in the actual limits derived from Ursa Minor between 100 GeV and 3 TeV (shown in Fig 10 bottom left), and that at the 10 GeV range we consider -using the $b\bar{b}$ channel- those limits to be consistent to that of [51] for the same dSph. For Sextans our limits compared to those of [51], are at the TeV range a factor of 2 stronger. At low masses, as is shown in Fig. 10 (bottom right) it is unsafe to make a claim based on the robustness of these limits. Finally, when comparing our strongest limits from Ursa Minor to the limits from the joint likelihood of [51], we get that our constraints between m_χ of 100 GeV and 1 TeV are a factor of 2 to 3 weaker for all channels. Between m_χ of 10-100 GeV the relative difference of our limits to those of [51] fluctuates for $b\bar{b}$ and $\tau^+\tau^-$ with our limits being slightly tighter at 10 GeV. For the $\mu^+\mu^-$ channel our limits remain always a factor of 2 more weak.

Limits from VERITAS [125, 126] are most competitive at the TeV range of masses. Yet even at $m_\chi = 1$ TeV, our limits are tighter by a factor of 10 (for the $b\bar{b}$ channel). Limits from MAGIC-I telescope [127, 128] give slightly weaker limits to those of VERITAS but are expected to get more competitive with MAGIC-II up-grate [129, 130].

Given that in our analysis we study separately each dSph galaxy/target in order to understand the robustness of the DM annihilation limits derived and then based *only* on the targets that give the most robust limits, claim constraints on DM annihilation rates, our results are safer, while providing also similarly tight limits. Since in our process it is of equal importance, to understand well the relevant uncertainties on the J-factors, we have left the study of dSphs such as the Ursa Magor II, Seque I and Coma Berenices for future work where the uncertainty in the relevant J-factors is well modeled.

In Fig. 12 (left), we also give the 68% to 99.9% CL limits for $\chi\chi \longrightarrow W^+W^-$. We note that the 99.9% CL are only by a factor of 2 more stringent than the 68% for both dSphs. We show limits using either only the PYTHIA simulation without final state radiation (FSR), with FSR (used in Fig. 8-10) and including electroweak (EW) (Fig. 11)corrections.
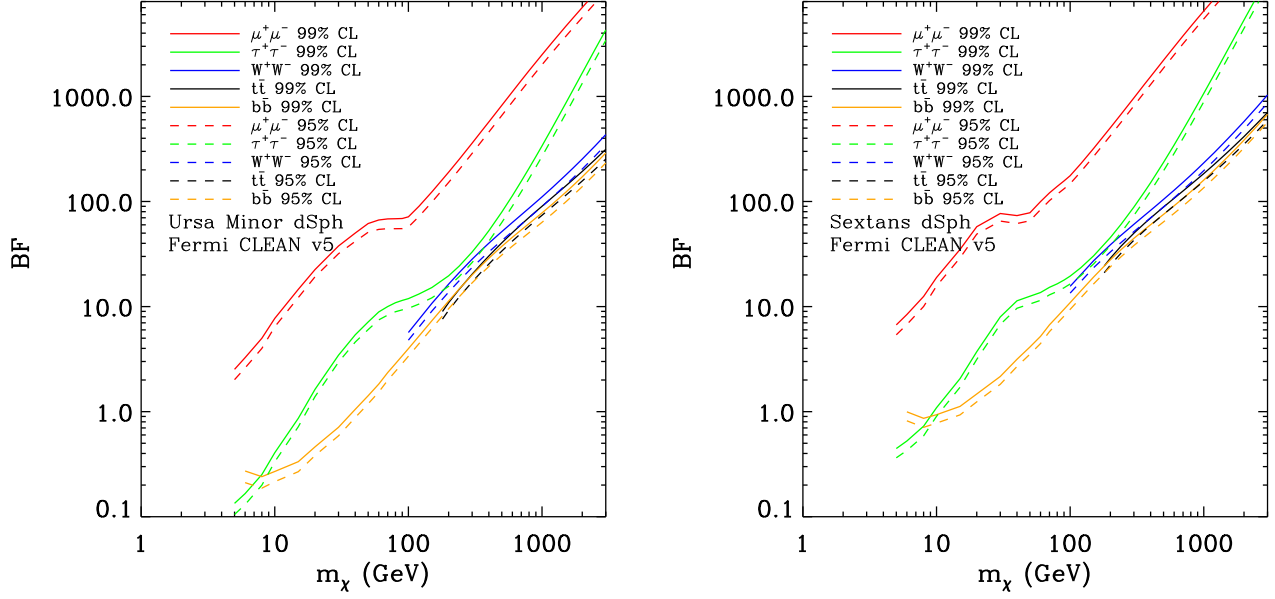
FIG. 11: 99% and 95% C.L. limits from Ursa Minor (*left*) and Sextans (*right*) for different annihilation channels. Red: $\chi\chi \longrightarrow \mu^+\mu^-$, green: $\chi\chi \longrightarrow \tau^+\tau^-$, orange: $\chi\chi \longrightarrow b\bar{b}$, blue: $\chi\chi \longrightarrow W^+W^-$, black: $\chi\chi \longrightarrow t\bar{t}$.

For the W^+W^- channel, the difference between the three cases of prompt γ-ray spectra calculation, is not significant. Yet as we show in Fig. 12 (right), EW corrections are more important for channels as the leptonic ones, as is the $\mu^+\mu^-$ (see also discussion in [114, 116, 124, 131]).

While our limits from Ursa Minor are slightly weaker than the joint likelihood of [51], they are still stronger than limits using γ-rays at medium and high latitudes [132] and can put constraints on DM at γ-rays from regions sarounding the GC where an annihilation signal may lay especially in the leptophilic DM case [132–135].

Limits from the galactic center region [105, 132, 135–137] are more competitive above 100 GeV, but suffer strongly form uncertainties in the exact profile assumed and for the Sommerfeld enhancement cases also from the different velocity dispersion locally than in the GC [21] and the extend of DM substructures in the Galaxy [138, 139]. A case of a DM particle with mass ≈ 10 GeV annihilating mainly into leptons [140–142] to account for the suggested excess of γ-rays towards the GC [140], can not be ruled out since as we described in section III our limits bellow $m_\chi < 10$ GeV depend only on the low energy γ-ray bins and are more sensitive to background assumptions.

Observations of galaxy clusters at γ-rays have also given limits on annihilating DM [143–145] which though in some cases are stronger, depend greatly (up to 3 orders of magnitude in the strength of the limits [145]) on the significance of substructure in the outer parts of the clusters and also on taking into account the γ-ray production from SM particles, which is significant for those targets of DM annihilation signals.

Finally limits on DM annihilation from antiprotons [23–26], are sensitive on galactic propagation assumptions [26]. Yet when comparing to limits assuming conventional propagation assumptions our limits for the $\chi\chi \longrightarrow W^+W^-$, $b\bar{b}$ are weaker at ≈ 100 GeV and as strong as at 1 TeV, as those from antiprotons. Also for the $\chi\chi \longrightarrow \mu^+\mu^-$ including EW corrections that are responsible for the emission of $\bar{p}$[114, 124] our limits are comparable to those from antiprotons [26] above a TeV.

VI. CONCLUSIONS

In this work we have revisited the constraints on DM annihilation from dSph galaxies which have been claimed to provide very tight limits on DM annihilation cross-sections [50, 51].

In doing so, we have discussed why cored DM halo profiles are preferable to the NFW profile, or in general cuspy profiles for dSphs. The main argument in favor of the cored profiles comes from observations as we discussed in section II. There is also theoretical motivation though: some early strong outflow event depleted the region of the dSphs from baryons suppressing also the baryonic infall at later stages, thus making the dSphs less cuspy than standard galaxies or galaxy clusters [146], suggested also by observations. Choosing the correct DM profile can have a
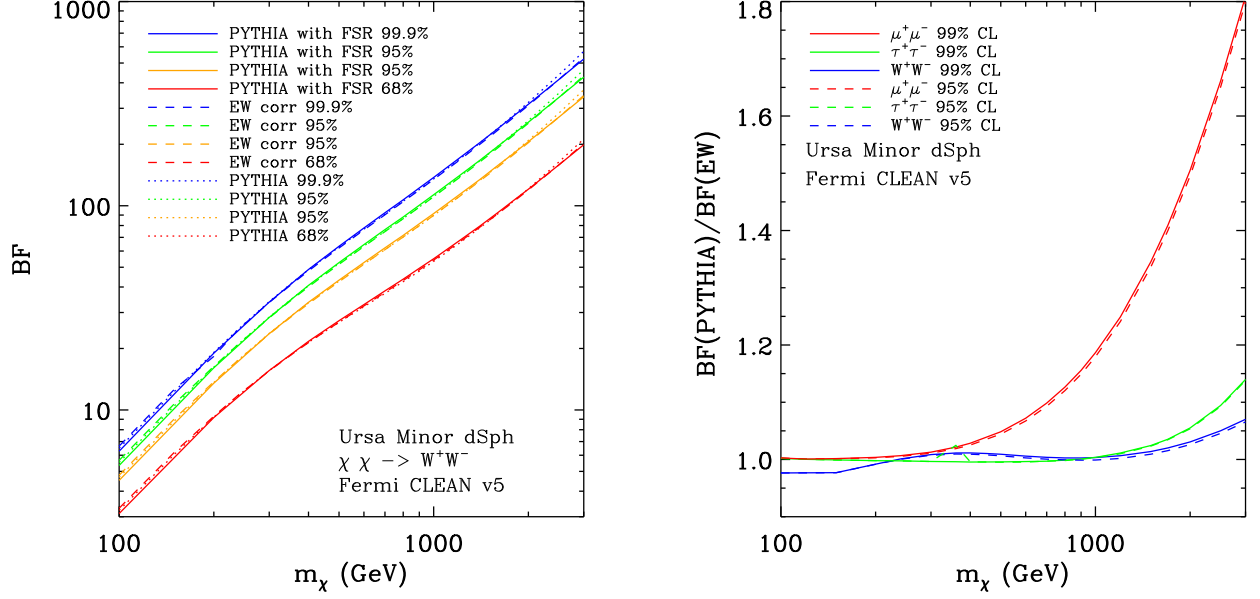
FIG. 12: *Left*: limits from Ursa Minor, on DM annihilation to W^+W^-, *blue* 99.9%, *green*: 99%, *orange*: 95% and *red*: 68% C.L. using *Fermi* CLEAN class data. *Solid lines*: PYTHIA with FSR, *dotted lines*: PYTHIA without FSR, *dashed lines*: including EW corrections. *Right*: for channels of DM annihilation to $\mu^+\mu^-$, $\tau^+\tau^-$ and W^+W^- we show the ratio of limits using the PYTHIA spectra to the limits using EW corrected spectra.

result on the limits on DM annihilation cross-sections vs mass that are usually presented. What we actually observe and constrain is the total annihilation rate which is proportional to the product of the annihilation cross-section and the J-factor that accounts for the observed DM annihilation profile integrated along the lines of sight within the observation angular window.

Apart from the profile itself, in setting the correct limits on DM annihilation cross-section it is also important to have a good understanding of the relevant uncertainty in the J-factors, which in many cases of dSphs is not insignificant. We choose to study eight dSphs for which we have accurate measurements of both the J-factors and their errors [89]; namely Carina, Draco, Fornax, Leo I, Leo II, Sculptor, Sextans and Ursa Minor.

For every target we model the background using alternative methods, in order to discriminate targets for which we have good understanding of the background and can give robust residuals leading to robust limits on DM annihilation.

All alternative background estimation/residual estimation methods, avoid having many degrees of freedom that could result in hiding any small excess. The only degrees of freedom are actually related to the borders of the regions of interest. These in turn are related (as are the borders of the signal ROIs) to the PSF at different energies. In fact we use we use the fact that all dSphs are practically point sources, thus their size (which defines the size of the signal ROIs) is *not* constant but depends sensitively on the energy of the observed γ-rays. By using γ-rays with energies between 1 and 100 GeV we can avoid having low energy γ-rays dominating our results. Above 100 GeV very few photons are observed around each dSph. In extracting residuals our methods cancel out the CR contamination and isotropic gamma-rays components, which at higher latitudes and energies can be significant leaving only their Poisson noise to have an impact on our limits.

Having calculated our residual spectra from alternative methods, by comparing them, we can find for which dSphs close-by (in angle) point sources and galactic diffuse features can be significant in setting DM limits. The dSphs for which by changing among alternative methods (alternative choices for the ROIs), the limits on DM annihilating change dramatically (see Figs. 9 and 10) are excluded from further analysis. For such targets a physical model properly accounting for the γ-ray fluxes from point sources and galactic diffuse features is necessary. Such targets that are excluded are Draco and Sculptor dSphs even though they do provide tight limits in some cases.

Among the "clean" background dSph galaxies that we studied, Ursa Minor provides the best target to set robust and tight limits on DM annihilation. We give limits for $\chi\chi \longrightarrow t\bar{t}$, W^+W^-, $b\bar{b}$, $\tau^+\tau^-$ and $\mu^+\mu^-$ annihilation channels, shown in Fig. 11. Our limits form Ursa Minor are stronger than those of [51] for Ursa Minor by a factor of 5 (at DM mass $m_\chi \approx 10$ GeV) to 2 at $m_\chi \approx 1$ TeV for $\chi\chi \longrightarrow b\bar{b}$. When comparing our limits from Ursa Minor to those from the joint likelihood of [51] then we get comparable limits at 10 GeV for the $b\bar{b}$, $\tau^+\tau^-$ channels, a factor of 2 weaker

limits for the $\mu^+\mu^-$ channel and a factor of 2-3 weaker limits for all channels above 100 GeV. Yet the joint likelihood method does not take into account our arguments about robustness of DM limits between the individual targets.

Finally dSph galaxies such as Ursa Major II, Seque I and Coma Berenices are possibly the most interesting targets among those not discussed in this paper, to look for future work. Such a work will have to include for them as well, accurate estimates on the J-factors best values and uncertainties.

Acknowledgments

[1] M. Boezio et al. (2008), 0810.3508.
[2] O. Adriani et al. (PAMELA), Nature **458**, 607 (2009), 0810.4995.
[3] O. Adriani et al., Phys. Rev. Lett. **102**, 051101 (2009), 0810.4994.
[4] F. Aharonian et al. (H.E.S.S.), Phys. Rev. Lett. **101**, 261104 (2008), 0811.3894.
[5] F. Aharonian et al. (H.E.S.S.), Astron. Astrophys. **508**, 561 (2009), 0905.0105.
[6] A. A. Abdo et al. (The Fermi LAT), Phys. Rev. Lett. **102**, 181101 (2009), 0905.0025.
[7] J. Chang et al., Nature **456**, 362 (2008).
[8] N. Arkani-Hamed, D. P. Finkbeiner, T. R. Slatyer, and N. Weiner, Phys. Rev. **D79**, 015014 (2009), 0810.0713.
[9] I. Cholis, D. P. Finkbeiner, L. Goodenough, and N. Weiner, JCAP **0912**, 007 (2009), 0810.5344.
[10] R. Harnik and G. D. Kribs, Phys.Rev. **D79**, 095007 (2009), 0810.5557.
[11] Y. Bai and Z. Han, Phys.Rev. **D79**, 095023 (2009), 0811.0387.
[12] P. J. Fox and E. Poppitz, Phys.Rev. **D79**, 083528 (2009), 0811.0399.
[13] P. Grajek, G. Kane, D. Phalen, A. Pierce, and S. Watson, Phys.Rev. **D79**, 043506 (2009), 0812.4555.
[14] M. Pospelov and A. Ritz, Phys.Lett. **B671**, 391 (2009), 0810.1502.
[15] J. D. March-Russell and S. M. West, Phys.Lett. **B676**, 133 (2009), 0812.0559.
[16] M. Cirelli and A. Strumia, New J.Phys. **11**, 105005 (2009), 0903.3381.
[17] W. Shepherd, T. M. Tait, and G. Zaharijas, Phys.Rev. **D79**, 055022 (2009), 0901.2125.
[18] D. J. Phalen, A. Pierce, and N. Weiner, Phys.Rev. **D80**, 063513 (2009), 0901.3165.
[19] D. Hooper and K. M. Zurek, Phys.Rev. **D79**, 103529 (2009), 0902.0593.
[20] H.-S. Goh, L. J. Hall, and P. Kumar, JHEP **0905**, 097 (2009), 0902.0814.
[21] I. Cholis and N. Weiner (2009), 0911.4954.
[22] D. Hooper and T. M. Tait, Phys.Rev. **D80**, 055028 (2009), 0906.0362.
[23] M. Cirelli, M. Kadastik, M. Raidal, and A. Strumia, Nucl.Phys. **B813**, 1 (2009), 0809.2409.
[24] F. Donato, D. Maurin, P. Brun, T. Delahaye, and P. Salati, Phys. Rev. Lett. **102**, 071301 (2009), 0810.5292.
[25] I. Cholis, JCAP **1109**, 007 (2011), 1007.1160.
[26] C. Evoli, I. Cholis, D. Grasso, L. Maccione, and P. Ullio, Phys.Rev. **D85**, 123511 (2012), 1108.0664.
[27] L. Bergstrom, J. Edsjo, and G. Zaharijas, Phys.Rev.Lett. **103**, 031103 (2009), 0905.0333.
[28] L. Baudis, J. Phys. Conf. Ser. **65**, 012015 (2007), astro-ph/0703183.
[29] P. Barbeau, J. Collar, and O. Tench, JCAP **0709**, 009 (2007), submitted to Phys. Rev. C, nucl-ex/0701012.
[30] E. Aprile, L. Baudis, and f. t. X. Collaboration, PoS **IDM2008**, 018 (2008), 0902.4253.
[31] Z. Ahmed et al. (The CDMS-II Collaboration), Science **327**, 1619 (2010), 0912.3592.
[32] R. Bernabei et al. (DAMA), Nucl. Instrum. Meth. **A592**, 297 (2008), 0804.2738.
[33] G. Angloher, M. Bauer, I. Bavykina, A. Bento, A. Brown, et al. (2008), 0809.1829.
[34] J. Angle et al., Phys. Rev. Lett. **101**, 091301 (2008), 0805.2939.
[35] J. Kopp, T. Schwetz, and J. Zupan, JCAP **1002**, 014 (2010), 0912.4264.
[36] R. Bernabei et al., Eur. Phys. J. **C67**, 39 (2010), 1002.1028.
[37] E. Aprile et al. (XENON100 Collaboration), Phys.Rev.Lett. **105**, 131302 (2010), 1005.0380.
[38] C. Aalseth et al. (CoGeNT collaboration), Phys.Rev.Lett. **106**, 131301 (2011), 1002.4703.
[39] C. Aalseth, P. Barbeau, J. Colaresi, J. Collar, J. Diaz Leon, et al., Phys.Rev.Lett. **107**, 141301 (2011), published version, slightly expanded discussion of ROI uncertainties, one reference added, 1106.0650.
[40] G. Angloher, M. Bauer, I. Bavykina, A. Bento, C. Bucci, et al. (2011), 1109.0702.
[41] J. I. Collar and D. N. McKinsey (2010), 1005.0838.
[42] P. J. Fox, J. Kopp, M. Lisanti, and N. Weiner, Phys.Rev. **D85**, 036008 (2012), 28 pages, 14 figures, 3 tables/ version 2 has minor clarifications in the text, 1107.0717.
[43] D. Hooper and C. Kelso, Phys.Rev. **D84**, 083001 (2011), 1106.1066.
[44] A. Fitzpatrick, D. Hooper, and K. M. Zurek, Phys.Rev. **D81**, 115005 (2010), 16 pages, 14 figures. v2: references added, fig 4 and surrounding discussion modified., 1003.0014.

[45] S. Chang, J. Liu, A. Pierce, N. Weiner, and I. Yavin, JCAP **1008**, 018 (2010), 1004.0697.
[46] S. Chang, N. Weiner, and I. Yavin, Phys.Rev. **D82**, 125011 (2010), 1007.4200.
[47] M. R. Buckley, D. Hooper, and T. M. Tait, Phys.Lett. **B702**, 216 (2011), 1011.1499.
[48] A. V. Belikov, J. F. Gunion, D. Hooper, and T. M. Tait, Phys.Lett. **B705**, 82 (2011), 6 pages, published version, 1009.0549.
[49] E. Del Nobile, C. Kouvaris, and F. Sannino, Phys.Rev. **D84**, 027301 (2011), 1105.5431.
[50] A. Abdo, M. Ackermann, M. Ajello, W. Atwood, L. Baldini, et al., Astrophys.J. **712**, 147 (2010), 1001.4531.
[51] M. Ackermann et al. (Fermi-LAT collaboration), Phys.Rev.Lett. **107**, 241302 (2011), 1108.3546.
[52] N. W. Evans, F. Ferrer, and S. Sarkar, Phys. Rev. D **69**, 123501 (2004), arXiv:astro-ph/0311145.
[53] S. Colafrancesco, S. Profumo, and P. Ullio, Phys.Rev. **D75**, 023513 (2007), astro-ph/0607073.
[54] L. E. Strigari, S. M. Koushiappas, J. S. Bullock, and M. Kaplinghat, Phys.Rev. **D75**, 083526 (2007), astro-ph/0611925.
[55] J. Bovy, Phys.Rev. **D79**, 083539 (2009), 0903.0413.
[56] P. Scott, J. Conrad, J. Edsjo, L. Bergstrom, C. Farnier, et al., JCAP **1001**, 031 (2010), 0909.3300.
[57] M. Perelstein and B. Shakya, JCAP **1010**, 016 (2010), 1007.0018.
[58] M. Persic, P. Salucci, and F. Stel, Mon. Not. R. Astron. Soc. **281**, 27 (1996), arXiv:astro-ph/9506004.
[59] P. Salucci, A. Lapi, C. Tonini, G. Gentile, I. Yegorova, and U. Klein, Mon. Not. R. Astron. Soc. **378**, 41 (2007), arXiv:astro-ph/0703115.
[60] W. J. G. de Blok, F. Walter, E. Brinks, C. Trachternach, S.-H. Oh, and R. C. Kennicutt, Jr., Astron. J. **136**, 2648 (2008), 0810.2100.
[61] L. Chemin, W. J. G. de Blok, and G. A. Mamon, Astron. J. **142**, 109 (2011), 1109.4247.
[62] G. Gentile, P. Salucci, U. Klein, D. Vergani, and P. Kalberla, Mon. Not. R. Astron. Soc. **351**, 903 (2004), arXiv:astro-ph/0403154.
[63] G. Gentile, A. Burkert, P. Salucci, U. Klein, and F. Walter, Astrophys. J. Lett. **634**, L145 (2005), arXiv:astro-ph/0506538.
[64] G. Gentile, P. Salucci, U. Klein, and G. L. Granato, Mon. Not. R. Astron. Soc. **375**, 199 (2007), arXiv:astro-ph/0611355.
[65] J. Kormendy, Astrophys. J. **295**, 73 (1985).
[66] A. Burkert, Astrophys. J. Lett. **447**, L25 (1995), arXiv:astro-ph/9504041.
[67] J. Kormendy and K. C. Freeman, in *Dark Matter in Galaxies*, edited by S. Ryder, D. Pisano, M. Walker, & K. Freeman (2004), vol. 220 of *IAU Symposium*, p. 377, arXiv:astro-ph/0407321.
[68] P. Salucci and A. Burkert, Astrophys.J. **537**, L9 (2000), astro-ph/0004397.
[69] J. Peñarrubia, A. W. McConnachie, and J. F. Navarro, Astrophys. J. **672**, 904 (2008), arXiv:astro-ph/0701780.
[70] M. G. Walker, M. Mateo, and E. W. Olszewski, Astron. J. **137**, 3100 (2009), 0811.0118.
[71] J. Kleyna, M. I. Wilkinson, N. W. Evans, G. Gilmore, and C. Frayn, Mon. Not. R. Astron. Soc. **330**, 792 (2002), arXiv:astro-ph/0109450.
[72] M. L. Mateo, Annu. Rev. Astron. Astrophys. **36**, 435 (1998), arXiv:astro-ph/9810070.
[73] G. Gilmore, M. I. Wilkinson, R. F. G. Wyse, J. T. Kleyna, A. Koch, N. W. Evans, and E. K. Grebel, Astrophys. J. **663**, 948 (2007), arXiv:astro-ph/0703308.
[74] A. Koch, M. I. Wilkinson, J. T. Kleyna, G. F. Gilmore, E. K. Grebel, A. D. Mackey, N. W. Evans, and R. F. G. Wyse, Astrophys. J. **657**, 241 (2007), arXiv:astro-ph/0611372.
[75] L. E. Strigari, J. S. Bullock, M. Kaplinghat, J. D. Simon, M. Geha, B. Willman, and M. G. Walker, Nature (London) **454**, 1096 (2008), 0808.3772.
[76] M. G. Walker, M. Mateo, E. W. Olszewski, J. Peñarrubia, N. Wyn Evans, and G. Gilmore, Astrophys. J. **704**, 1274 (2009), 0906.0341.
[77] R. R. Muñoz, S. R. Majewski, S. Zaggia, W. E. Kunkel, P. M. Frinchaboy, D. L. Nidever, D. Crnojevic, R. J. Patterson, J. D. Crane, K. V. Johnston, et al., Astrophys. J. **649**, 201 (2006), arXiv:astro-ph/0605098.
[78] A. Koch, J. T. Kleyna, M. I. Wilkinson, E. K. Grebel, G. F. Gilmore, N. W. Evans, R. F. G. Wyse, and D. R. Harbeck, Astron. J. **134**, 566 (2007), 0704.3437.
[79] G. Battaglia, A. Helmi, E. Tolstoy, M. Irwin, V. Hill, and P. Jablonka, Astrophys. J. Lett. **681**, L13 (2008), 0802.4220.
[80] M. G. Walker, M. Mateo, E. W. Olszewski, O. Y. Gnedin, X. Wang, B. Sen, and M. Woodroofe, Astrophys. J. Lett. **667**, L53 (2007), 0708.0010.
[81] J. F. Navarro, C. S. Frenk, and S. D. M. White, Astrophys. J. **490**, 493 (1997), arXiv:astro-ph/9611107.
[82] N. W. Evans, J. An, and M. G. Walker, Mon. Not. R. Astron. Soc. **393**, L50 (2009), 0811.1488.
[83] T. Goerdt, B. Moore, J. I. Read, J. Stadel, and M. Zemp, Mon. Not. R. Astron. Soc. **368**, 1073 (2006), arXiv:astro-ph/0601404.
[84] N. Amorisco and N. Evans, Mon.Not.Roy.Astron.Soc. **411**, 2118 (2011), 1009.1813.
[85] M. G. Walker and J. Penarrubia, Astrophys.J. **742**, 20 (2011), 1108.2404.
[86] G. Gentile, A. Burkert, P. Salucci, U. Klein, and F. Walter, Astrophys.J.Lett. (2005), astro-ph/0506538.
[87] A. V. Maccio', G. Stinson, C. B. Brook, J. Wadsley, H. Couchman, et al. (2011), 1111.5620.
[88] C. Ragone-Figueroa, G. L. Granato, and M. G. Abadi (2012), 1202.1527.
[89] P. Salucci, M. I. Wilkinson, M. G. Walker, G. F. Gilmore, E. K. Grebel, A. Koch, C. Frigerio Martins, and R. F. G. Wyse, Mon. Not. R. Astron. Soc. p. 2161 (2012), 1111.1165.
[90] J. Binney and S. Tremaine, *Galactic Dynamics: Second Edition* (Princeton University Press, 2008).
[91] G. A. Mamon and E. L. Łokas, Mon. Not. R. Astron. Soc. **363**, 705 (2005), arXiv:astro-ph/0405491.
[92] F. Donato, G. Gentile, P. Salucci, C. Martins, M. Wilkinson, et al. (2009), 0904.4054.
[93] A. Charbonnier, C. Combet, M. Daniel, S. Funk, J. Hinton, et al., Mon.Not.Roy.Astron.Soc. **418**, 1526 (2011), 1104.0412.

[94] A. Abramowski et al. (HESS Collaboration), Astropart.Phys. **34**, 608 (2011), 1012.5602.
[95] A. Abdo et al. (The Fermi-LAT collaboration), Phys.Rev.Lett. **104**, 101101 (2010), 1002.3603.
[96] A. W. Strong, I. V. Moskalenko, and O. Reimer, Astrophys. J. **613**, 962 (2004), astro-ph/0406254.
[97] I. Cholis, M. Tavakoli, C. Evoli, L. Maccione, and P. Ullio, JCAP **1205**, 004 (2012), 1106.5073.
[98] A. A. Abdo, M. Ackermann, M. Ajello, W. B. Atwood, M. Axelsson, L. Baldini, J. Ballet, G. Barbiellini, M. G. Baring, D. Bastieri, et al., Science **325**, 848 (2009).
[99] J. M. Siegal-Gaskins, R. Reesman, V. Pavlidou, S. Profumo, and T. P. Walker (2010), 1011.5501.
[100] F. Calore, V. De Romeri, and F. Donato, Phys.Rev. **D85**, 023004 (2012), 10 pages, 6 figures Version updated, as sent to PRD, 1105.4230.
[101] D. Malyshev, I. Cholis, and J. D. Gelfand, Astrophys.J. **722**, 1939 (2010), 1002.0587.
[102] The Fermi-LAT Collaboration, Astrophys.J.Suppl. **188**, 405 (2010), 1002.2280.
[103] The Fermi-LAT Collaboration (Fermi-LAT Collaboration), Astrophys.J.Suppl. **199**, 31 (2012), 1108.1435.
[104] A. A. Abdo et al. (Fermi LAT Collaboration), Astrophys.J.Suppl. **183**, 46 (2009), 0902.1340.
[105] A. Abramowski et al. (H.E.S.S.Collaboration), Phys.Rev.Lett. **106**, 161301 (2011), 1103.3266.
[106] F. Aharonian et al. (H.E.S.S. Collaboration), Nature **439**, 695 (2006), astro-ph/0603021.
[107] F. Aharonian et al. (H.E.S.S. Collaboration), Phys.Rev.Lett. **97**, 221102 (2006), astro-ph/0610509.
[108] http://www.sciops.esa.int/SA/PLANCK/docs/ERCSC_explanatory_supplement.pdf (2011).
[109] Planck Collaboration, P. A. R. Ade, N. Aghanim, M. Arnaud, M. Ashdown, J. Aumont, C. Baccigalupi, A. Balbi, A. J. Banday, R. B. Barreiro, et al., Astron. Astrophys. **536**, A7 (2011), 1101.2041.
[110] C. B. Haakonsen and R. E. Rutledge, Astrophys.J.Suppl. **184**, 138 (2009), 0910.3229.
[111] M. Shirahata, S. Matsuura, S. Hasegawa, T. Ootsubo, S. Makiuti, et al. (2009), 0904.3788.
[112] T. Sjostrand, S. Mrenna, and P. Z. Skands, JHEP **0605**, 026 (2006), hep-ph/0603175.
[113] K. N. et al., J. Phys. G 37, 075021 (2010) and 2011 partial update for the 2012 edition (2010).
[114] P. Ciafaloni, D. Comelli, A. Riotto, F. Sala, A. Strumia, et al., JCAP **1103**, 019 (2011), 1009.0224.
[115] A. Hryczuk and R. Iengo, JHEP **1201**, 163 (2012), 1111.2916.
[116] P. Ciafaloni, D. Comelli, A. De Simone, A. Riotto, and A. Urbano, JCAP **1206**, 016 (2012), 1202.0692.
[117] A. W. Strong, I. V. Moskalenko, and V. S. Ptuskin, Ann. Rev. Nucl. Part. Sci. **57**, 285 (2007), astro-ph/0701517.
[118] T. Delahaye, A. Fiasson, M. Pohl, and P. Salati, Astron. Astrophys. **531**, A37 (2011), 1102.0744.
[119] The Fermi-LAT Collaboration (Fermi-LAT Collaboration), Astrophys.J. **750**, 3 (2012), 1202.4039.
[120] H. Nakanishi and Y. Sofue, Publ.Astron.Soc.Jap. (2006), astro-ph/0610769.
[121] H. Nakanishi and Y. Sofue, Publ.Astron.Soc.Jap. **55**, 191 (2003), astro-ph/0304338.
[122] M. Pohl, P. Englmaier, and N. Bissantz, Astrophys. J. **677**, 283 (2008), 0712.4264.
[123] I. V. Moskalenko, S. Digel, T. Porter, O. Reimer, and A. Strong, Nucl.Phys.Proc.Suppl. **173**, 44 (2007), astro-ph/0609768.
[124] M. Cirelli, G. Corcella, A. Hektor, G. Hutsi, M. Kadastik, et al., JCAP **1103**, 051 (2011), 57 pages with many figures and tables. v2: several discussions and references added, some figures improved, matches version published on JCAP. v3: a few typos corrected and some references updated. All results are available at http://www.marcocirelli.net/PPPC4DMID.html, 1012.4515.
[125] Vivier, M. for the VERITAS Collaboration (2011), 1110.6615.
[126] E. Aliu et al. (VERITAS Collaboration), Phys.Rev. **D85**, 062001 (2012), 1202.2144.
[127] J. Aleksic et al. (The MAGIC Collaboration), JCAP **1106**, 035 (2011), 1103.0477.
[128] S. Paiano, S. Lombardi, M. Doro, D. Nieto, f. t. M. Collaboration, et al. (2011), 1110.6775.
[129] T. Bringmann, M. Doro, and M. Fornasa, JCAP **0901**, 016 (2009), 0809.2269.
[130] O. Tibolla (for the MAGIC collaboration) (2012), 1201.2295.
[131] A. De Simone (2012), 1201.1443.
[132] M. Cirelli, P. Panci, and P. D. Serpico, Nucl.Phys. **B840**, 284 (2010), 0912.0663.
[133] I. Cholis, G. Dobler, D. P. Finkbeiner, L. Goodenough, and N. Weiner, Phys. Rev. **D80**, 123518 (2009), 0811.3641.
[134] I. Cholis, G. Dobler, D. P. Finkbeiner, L. Goodenough, T. R. Slatyer, et al. (2009), 0907.3953.
[135] M. Papucci and A. Strumia, JCAP **1003**, 014 (2010), 0912.0742.
[136] P. Meade, M. Papucci, and T. Volansky, JHEP **0912**, 052 (2009), 0901.2925.
[137] K. N. Abazajian and J. Harding, JCAP **1201**, 041 (2012), 19 pages, 5 figures/ v3: Matches JCAP version/ includes discussion of numerical studies of the density profile of MW-type halos, updated references and comparisons, 1110.6151.
[138] I. Cholis and L. Goodenough, JCAP **1009**, 010 (2010), 1006.2089.
[139] T. R. Slatyer, N. Toro, and N. Weiner (2011), 17 pages, 7 figures, submitted to PRD. v2 adds the KITP preprint number and a comment on accelerator searches for light gauge bosons, 1107.3546.
[140] D. Hooper and L. Goodenough, Phys.Lett. **B697**, 412 (2011), 1010.2752.
[141] D. Hooper and T. Linden, Phys.Rev. **D84**, 123005 (2011), 13 pages, 11 figures, 1110.0006.
[142] D. Hooper (2012), 1201.1303.
[143] A. Pinzke, C. Pfrommer, and L. Bergstrom, Phys.Rev. **D84**, 123509 (2011), 43 pages, 23 figures, 10 tables. Accepted for publication in Phys. Rev. D: streamlined paper, added a paragraph about detectability to introduction, few references added, and few typos corrected, 1105.3240.
[144] S. Ando and D. Nagai, JCAP **1207**, 017 (2012), 1201.0753.
[145] J. Han, C. S. Frenk, V. R. Eke, L. Gao, and S. D. White (2012), 1201.1003.
[146] F. Governato, A. Zolotov, A. Pontzen, C. Christensen, S. Oh, et al., Mon.Not.Roy.Astron.Soc. **422**, 1231 (2012), 1202.0554.

[147] J. Hisano, S. Matsumoto, M. Nagai, O. Saito, and M. Senami, Phys.Lett. **B646**, 34 (2007), hep-ph/0610249.

[148] M. Lattanzi and J. I. Silk, Phys. Rev. **D79**, 083523 (2009), 0812.0360.

[149] A. Sommerfeld, Annalen der Physik **403**, 257 (1931).

[150] for a Majorana DM particle

[151] with the exception of Fornax and Draco where velocity dispersion data extend out to $\approx$1.5 kpc see Fig. 1 of [89]

[152] It is usual to stress that while many cored models are as really indistinguishable when compared to the observed kinematics in galaxies, for instance the Plummer profile, or some cases the pseudo-isothermal profile; the Zhao model sometimes used in modeling dSph is not the correct extrapolation of a NFW profile that gets a inner flat core. In fact, 1) 3 DM free parameters are to many in view of the qualitatively limited amount of information data available, the best fit solution is prone to bad degeneracies of the parameter values 2) in cored models (e.g. in spiral) there no support to the fact that the large scale and central DM density profiles are somewhat related, an unavoidable consequence of the Zhao model.

[153] See: http://www.slac.stanford.edu/exp/glast/groups/canda/lat_Performance.htm

[154] http://fermi.gsfc.nasa.gov/ssc/data/analysis/documentation/Pass7_usage.html

[155] http://fermi.gsfc.nasa.gov/ssc/data/analysis/scitools/

[156] For energies 100 MeV $< E_\gamma <$ 10 GeV the containment angle at normal incidence for SOURCE and CLEAN class is between $0.2° - 6°$ at 68% containment and $0.7° - 20°$ at 95% containment; being smaller at the higher energies. Between 10 and 100 GeV, the 68% (95%) containment angle varies much less, between $0.2° - 0.3°$ ($0.7° - 0.8°$), being again smaller at higher energies. See: http://www.slac.stanford.edu/exp/glast/groups/canda/lat_Performance.html for a plot and http://fermi.gsfc.nasa.gov/ssc/data/analysis/documentation/Cicerone/Cicerone_LAT_IRFs/IRF_PSF.html for parametric description for all classes and for front/backcoverted events.

[157] J1725 is not the brightest point source defined from the minimization procedure, as the one with the highest integrated flux for each case of assumptions on ROI and energy range.

[158] apart from its Poisson noise

[159] Draco from 4 p.s. to 15 p.s., Sextans from 4 p.s. to 13 p.s., Sculptor 1 p.s. for both cases, and Ursa Minor from 1 p.s. to 3 p.s.; with both cases though the total p.s. flux being a subdominant part of the background flux in the energy range of study.

[160] For the Sommerfeld enhancement case [8, 147–149], where the cross-section depends on the relative velocity between the DM particles, decoupling the annihilation cross-section from the DM profile, is not obvious. Yet since dSphs have low velocity dispersions, it may be the case that the cross-section has already reached saturation.

[161] It has been shown in calculations of DM annihilating in our Galaxy for cases as $\chi\chi \longrightarrow W^+W^-$, the γ-ray spectra of DM origin at energies close to the mass of the DM particle ($E_\gamma \sim m_\chi/3$) are dominated by the prompt γ-rays while for energies $E_\gamma \lesssim m_\chi/30$ the ICS and bremsstrahlung contribution become dominant (see for instance Fig. 1 of [101]).

[162] dSphs at low latitudes have been generally avoided in studies in order not to have too much galactic γ-ray contribution into the ROI.

[163] Only if all gas at high latitudes is local and taken as local can we trust the galactic diffuse γ-ray component. This is not always the case.